

CHARACTERIZATION OF PULSE OPERATION IN  
DEPRESSED-CLADDING ERBIUM DOPED FIBER LASER

NUR SABIRAH BINTI AZHARI

INSTITUTE OF GRADUATE STUDIES  
UNIVERSITY OF MALAYA  
KUALA LUMPUR

2016

**CHARACTERIZATION OF PULSE OPERATION IN  
DEPRESSED-CLADDING ERBIUM DOPED FIBER  
LASER**

**NUR SABIRAH BINTI AZHARI**

**DISSERTATION SUBMITTED IN FULFILMENT OF  
THE REQUIREMENTS FOR THE MASTER OF  
PHILOSOPHY**

**INSTITUTE OF GRADUATE STUDIES  
UNIVERSITY OF MALAYA  
KUALA LUMPUR**

**2016**

**UNIVERSITY OF MALAYA**  
**ORIGINAL LITERARY WORK DECLARATION**

Name of Candidate: Nur Sabirah binti Azhari

Registration/Matric No: HGG 130007

Name of Degree: Master of Philosophy

Title of Project Paper/Research Report/Dissertation/Thesis ("this Work"):

Characterization of Pulse Operation in Depressed-Cladding Erbium Doped Fiber  
Laser

Field of Study: Photonics Science

I do solemnly and sincerely declare that:

- (1) I am the sole author/writer of this Work;
- (2) This Work is original;
- (3) Any use of any work in which copyright exists was done by way of fair dealing and for permitted purposes and any excerpt or extract from, or reference to or reproduction of any copyright work has been disclosed expressly and sufficiently and the title of the Work and its authorship have been acknowledged in this Work;
- (4) I do not have any actual knowledge nor do I ought reasonably to know that the making of this work constitutes an infringement of any copyright work;
- (5) I hereby assign all and every rights in the copyright to this Work to the University of Malaya ("UM"), who henceforth shall be owner of the copyright in this Work and that any reproduction or use in any form or by any means whatsoever is prohibited without the written consent of UM having been first had and obtained;
- (6) I am fully aware that if in the course of making this Work I have infringed any copyright whether intentionally or otherwise, I may be subject to legal action or any other action as may be determined by UM.

Candidate's Signature

Date:

Subscribed and solemnly declared before,

Witness's Signature

Date:

Name:

Designation:

## ABSTRACT

There has been intense work on the pulse operation in the conventional (C-) band, long wavelength (L-) band as well as in the 2  $\mu\text{m}$  region. Nevertheless, as increasing demands for bandwidth have now pushed the envelope into the short-wavelength (S-band) region, it is of interest to further expand this coverage into the S-band region. In this research, depressed-cladding erbium doped fiber (DC-EDF) are chosen to accomplish S-band fiber laser because of their ability to provide and maintain high level of inversion along the fiber. It is designed with different index profile and this is called W-shape index profile. The system uses a 15 m long DC- EDF as a gain medium which is spooled with a diameter of about 9cm so as to inhibit operation at wavelengths of more than 1530 nm, while a thin CNT film is sandwiched between two connectors to function as the SA for the generation of the desired Q-switched pulses. To investigate the tunable Q-Switched fiber laser operating in the S-band region, a tunable Fabry-Perot etalon filter is inserted in the setup as the wavelength tuning and filtering mechanism. The tuning range of the laser output carrying the Q-switching pulses covers a wide wavelength range of 47 nm, which spans from 1479 nm to 1526 nm. In this research, we investigate and demonstrate the pulse operation in DC-EDF. To the best of our knowledge, this is the first demonstration of characterization pulse operation in S band region using DC-EDF.

## ABSTRAK

Terdapat banyak kajian mengenai operasi denyutan dalam gelombang jalur konvensional (C-band), gelombang jalur panjang (L-band) dan juga 2  $\mu\text{m}$ . Walau bagaimana pun, kini semakin meningkat kajian yang menjurus kepada gelombang jalur pendek (S-band). Dalam kajian ini, lapisan terhimpit gentian berdop erbium (DC-EDF) dipilih untuk mendapatkan laser gentian dalam jalur S kerana kemampuannya untuk menyediakan dan mengekalkan penyongsangan bertahap tinggi di sepanjang gentian. Ia direka dengan profil indeks yang berbeza yang dipanggil profil indeks bentuk W. Sistem ini menggunakan DC-EDF 15 m sebagai medium gandaan yang digulung dengan diameter kira-kira 9 cm bagi menghalang operasi pada jarak gelombang lebih daripada 1530nm. Manakala filem carbon nanotube (CNT) nipis diapit antara dua penyambung yang berfungsi sebagai penyerap tepu bagi menjana denyutan Suis-Q yang dikehendaki. Suis-Q boleh laras laser gentian di kawasan gelombang jalur pendek S pula dikaji dengan memasukkan penapis Fabri-Perot etalon ke dalam struktur eksperimen yang bertindak sebagai gelombang jalur boleh laras dan mekanisme penapisan. Rangkaian penalaan output laser yang membawa denyutan Q-suis meliputi julat panjang gelombang 47 nm, yang menjangkau dari 1479 nm hingga 1526 nm. Kajian ini menyiasat dan menunjukkan operasi denyutan dalam pelapisan tertekan gentian optik berdop erbium. Setakat ini, diketahui hanya ini merupakan demonstrasi pertama yang berkaitan dengan operasi denyutan di kawasan gelombang jalur S (S-band) yang menggunakan pelapisan tertekan gentian berdop erbium.

## ACKNOWLEDGEMENTS

Alhamdulillah. Praise to Allah for the chance to complete this dissertation. I would like to express my gratitude to my supervisors Dr. Mohd Zamani Zulkifli and Profesor Ulung Datuk Dr. Harith Ahmad for their full support, guidance, encouragement throughout my study and research. Without their wisdom and counsel, my dissertation would not been completed in time. In addition, I would like to express my appreciation to all the staff of Photonics Reseach Centre espeacialy Encik Faizal Ismail for their cooperation, commitment and time in making sure I could complete my research.

Special thanks also goes to my fellow friends for their understanding and support throughout this academic exploration. Without their support, this dissertation would have been a frustrating and overwhelming pursuit.

Finally, I would like to thank my parents, sister and brother for their prayers, unconditional love and support during the last two years. I would not have been able to complete this dissertation without their continuous love and encouragement. Thank you.

## TABLE OF CONTENTS

Abstract .....	iii
Abstrak .....	iv
Acknowledgements .....	v
Table of Contents .....	vi
List of Figures .....	ix
List of Symbols and Abbreviations.....	xi
<b>CHAPTER 1: INTRODUCTION.....</b>	<b>1</b>
1.1 Introduction .....	1
1.2 Problem statement .....	4
1.3 Thesis objective .....	4
1.4 Thesis arrangement .....	4
<b>CHAPTER 2: LITERATURE REVIEW.....</b>	<b>6</b>
2.1 Introduction .....	6
2.2 Fiber laser developments .....	6
2.3 S-band fiber laser .....	13
2.4 Depressed-cladding erbium doped fiber laser .....	14
2.5 Pulse operation .....	17
2.5.1 Q-switched.....	18
2.6 Fabry–Perot etalon filter .....	21
2.7 Carbon nanotube .....	22
2.7.1 Fabrication of CNT-based photonics devices .....	26
2.7.2 Saturable Absorption.....	26

<b>CHAPTER 3: METHODOLOGY .....</b>	<b>30</b>
3.1 Introduction .....	30
3.2 Optical devices used in the experiments .....	30
3.2.1 Laser Diode .....	30
3.2.2 Wavelength division multiplexing .....	31
3.2.3 Optical isolator .....	32
3.2.4 Couplers.....	34
3.2.5 Fiber Bragg Gratings .....	35
3.2.6 Faraday rotator mirror .....	37
3.3 To characterize pulsed operation in depressed-cladding erbium doped fiber laser... ..	39
3.4 To study the wavelength range tunability of Q-switched operation in the S-band region .....	41
3.5 SLM Distributed Bragg Reflector Fiber Laser using DC-EDF.....	42
<b>CHAPTER 4: RESULTS AND DISCUSSION .....</b>	<b>43</b>
4.1 Introduction .....	43
4.2 Q-Switched S-band Fiber laser .....	43
4.3 Tunable Q-switched DC-EDF laser using CNT by Fabry-Perot etalon filter .....	47
4.4 SLM Distributed Bragg Reflector Fiber Laser using DC-EDF.....	52
<b>CHAPTER 5: CONCLUSION.....</b>	<b>57</b>
5.1 Conclusion .....	57
5.2 Future works .....	57
References .....	59
List of Publications .....	70

University of Malaya

## LIST OF FIGURES

Figure 2.1: Illustration of three different laser cavities: (A) conventional resonant cavity, (B) one reflector cavity and (C) random cavity .....	9
Figure 2.2: Depressed cladding fibre cross-sectional view.....	15
Figure 2.3: W-Profile of Single Mode fiber .....	16
Figure 2.4: Fabry-Perot etalon filter from Micron Optic .....	21
Figure 2.5: Fabry-Perot interferometer, with $P_i$ , $P_r$ , and $P_t$ the incident, reflected, and transmitted optical power, respectively.....	21
Figure 2.6: Absorption spectra of a SWNT-PC composite and pure PC. The stripes show the telecommunication windows that can be potentially covered by this composite. S band: 1460-1530 nm, C band:1530-1565 nm, L band: 1565-1625 nm and U band: 1625-1675 nm.....	28
Figure 3.1: TEC laser diode.....	30
Figure 3.2: wavelength division multiplexing.....	31
Figure 3.3: Schematic structure of ordinary optical isolator.....	33
Figure 3.4: A simple 1X2 coupler with one input and two outputs.....	34
Figure 3.5: An Expanded View of an FBG.....	35
Figure 3.6: Setup of a double-pass laser amplifier that includes the Faraday mirror.....	37
Figure 3.7: Experimental setup of the proposed Q-switched S-band fiber laser.....	39
Figure 3.8: Experimental setup of the proposed tunable Q-switched S-band fiber.....	40
Figure 3.9: Experimental setup for the SLM DBR fiber laser using DC-EDF.....	41
Figure 4.1: Output power as a function of pump power.....	43
Figure 4.2: Output spectrum of the proposed Q-switched S-band fiber laser.....	44
Figure 4.3: Repetition rate and pulse width against pump power.....	45
Figure 4.4: Output pulse train at wavelength of 1499 nm with repetition rate value of 25.9 kHz.....	46

Figure 4.5: Repetition rate against wavelength.....	47
Figure 4.6: (a) Output spectra of the proposed system for 11 tuned wavelengths at an interval of 5 nm (b) Zoom in view of the output spectra at a wavelength interval of 1 nm.....	48
Figure 4.7: Output pulse train at wavelength of 1509 nm with repetition rate value of 26.5 kHz.....	49
Figure 4.8: Pulse Energy against wavelength.....	50
Figure 4.9: Output spectrum of the SLM DBR fiber laser with different pump power.....	51
Figure 4.10: Zoom in view of output spectrum in Figure 4.9.....	52
Figure 4.11: Stability measurement of the output laser.....	53
Figure 4.12: Average output power against pump power.....	53
Figure 4.13: RFSA spectrum of the output laser by the SLM DBR fiber laser setup...54	
Figure 4.14: Delayed self-heterodyned technique using a Mach-Zehnder interferometer (MZI).....	55
Figure 4.15: RF spectrum of delayed self-heterodyne signal.....	55

## LIST OF SYMBOLS AND ABBREVIATIONS

DC-EDF	:	Depressed-cladding erbium doped fiber
CNT	:	Carbon nanotube
CW	:	Continuous wave
Er <sup>3+</sup>	:	Erbium 3+
MCVD	:	Modified chemical vapor deposition
DWDM	:	Dense Wavelength Division Multiplexing
TDFAs	:	Thulium-doped fiber amplifiers
DCF	:	Dispersion compensating fiber
EDFAs	:	Erbium Doped Fiber Amplifiers
EDF	:	Erbium Doped Fiber
ASE	:	Amplified Spontaneous Emission
SMF-28	:	Single mode fiber
SESAMs	:	Saturable absorber mirrors
SA	:	Saturable absorbers
IR	:	Infrared
TFBG	:	Tunable fiber Bragg gratings
SWNTs	:	Single-wall nanotubes
s-SWNTs	:	Semiconducting SWNTs
m-SWNTs	:	Metallic SWNTs
PL	:	Photoluminescence
LD	:	Laser diode
WDM	:	Wavelength division multiplexer
OSA	:	Optical spectrum analyzer

FBG	:	Fiber bragg grating
DBR	:	Distributed Bragg reflector
FRM	:	Faraday reflector mirror
SLM	:	Single longitudinal mode
AOM	:	Acoustic optic modulator

University of Malaya

University of Malaya

## CHAPTER 1: INTRODUCTION

### 1.1 Introduction

A fiber laser is constructed using optical fiber doped with rare-earth elements such as erbium, ytterbium, thulium and neodymium as the gain medium. Fiber laser has inherent advantages that override the traditional solid state lasers. Among its advantages is the flexible structure of optical fiber which allows the laser in the fiber to be delivered easily to a focusing element. This is significant for laser welding, laser cutting, and folding of metals and polymers. Optical fiber lasers have higher optical quality and reliability low than solid state lasers and they are physically much more compact in size. A laser can be divided into two types, either operating in continuous or pulsed mode, depending on whether the power output is essentially continuous over time or whether its output takes the form of pulses of light on one or another time scale.

Some applications of lasers depend on a beam whose output power is constant over time. Such a laser is known as continuous wave (CW). For CW operation it is required for the population inversion of the gain medium to be continually replenished by a steady pump source. In some lasing media this is impossible. In some other lasers it would require pumping the laser at a very high continuous power level which would be impractical or destroy the laser by producing excessive heat. Such lasers cannot be run in CW mode. Pulsed operation of lasers refers to any laser not classified as continuous wave, so that the optical power appears in pulses of some duration at some repetition rate. In other cases the application requires the production of pulses having as large an energy as possible. Since the pulse energy is equal to the average power divided by the repetition rate, this goal can sometimes be satisfied by lowering the rate of pulses so that more energy can be built up in between pulses.

Q-switching and mode-locking are the two main techniques enabling pulsed lasers (Svelto, 1998). In mode-locking, the random phase relation originating from the interference of cavity modes is fixed, resulting in a single pulse (Svelto, 1998), with typical duration ranging from tens ps to sub-10 fs (U. Keller et al., 1996), and a repetition rate corresponding to the inverse of the cavity round-trip time (U. Keller et al., 1996). Many aspects, including the dispersive and nonlinear properties of the intracavity components, need to be precisely balanced in order to achieve stable operation (U. Keller et al., 1996; Svelto, 1998). Q-switching is a modulation of the quality factor,  $Q$ , of a laser cavity (Svelto, 1998),  $Q$  being the ratio between the energy stored in the active medium and that lost per oscillation cycle (Svelto, 1998) thus, the lower the losses, the higher the  $Q$ . In Q-switching, the active medium is pumped while lasing is initially prevented by a low  $Q$  factor (Svelto, 1998). The stored energy is then released in a pulse with duration ranging from  $\mu\text{s}$  to ns when lasing is allowed by a high  $Q$  factor (Svelto, 1998). The time needed to replenish the extracted energy between two consecutive pulses is related to the lifetime of the gain medium, which is typically  $\mu\text{s}$  for erbium-doped fibers (Svelto, 1998). Thus the repetition rate of Q-switched lasers is usually low  $\sim\text{kHz}$ , much smaller than mode-locked lasers (U. Keller et al., 1996; Svelto, 1998).

Fiber lasers are well known and widely used in industry because of their high power and relative simplicity. They find applications as industrial cutting or welding tools (Hausken, 2008; Masson, St-Gelais, Poulin, & Peter, 2010). Tunable fiber lasers are also good candidates as test and measurement sources for optical devices characterization because of their small spectral width, continuous tuning, and stability (Bellemare et al., 2001). Wide band gain of erbium enables tuning of  $\text{Er}^{3+}$  fiber laser over the whole telecommunication C and L-bands (Buck, 2004). Moreover, large  $\text{Er}^{3+}$

gain offers the opportunity to build powerful lasers or to use lossy photonic components in the laser cavity for tuning purposes (Digonnet, 2001).

The DC-EDF is fabricated using a standard modified chemical vapor deposition (MCVD) process with standard solution doping (Harun, Dimiyati, Jayapalan, & Ahmad, 2007) with insertion of fluorine into the depressed cladding. The DC-EDF is surrounded by a secondary cladding and has a core with a circular-cross section. This circular cross-section is also present in the depressed cladding and secondary cladding with the depressed cladding cross-section larger than core cross section. In the DC-EDF ions of the rare earth erbium are doped into the core of the fiber. These erbium ions act as a lasing medium and exhibit high gain at the C and L- band region. In order to obtain the S-band fiber laser by using the DC-EDF, the fundamental mode cutoff wavelength must be between the S-band and the long wavelength bands of the C- and L-band region. In particular the fundamental mode cutoff wavelength due to be S-band signal that remains in the core (M. A. Arbore, Zhou, & Kmetec, 2005) is preferably set near 1530 nm (Mark A. Arbore, 2005; Foroni et al., 2005). The fundamental mode cutoff can be determined by adjusting the cross section and refractive indices of core, depressed cladding and secondary cladding. The adjustment to the fundamental mode cut-off can also be made by adjusting the spooling diameter of the DC-EDF. Thus, by using fiber spools of varying diameters, the effect of the spool diameter on the fundamental mode cutoff of the DC-EDF can be observed in the study of the S-band DC-EDF. As well as the fundamental mode cutoff, other important parameters of the DC-EDF related to the spooling diameter can also be observed, such as the attenuation of the fiber due to the bending loss and the variation in the gain and noise figure of the S-band DC-EDF. These factors are critical in the development of compact DC-EDFs, as the size of the DC-EDF must have no detrimental effect on the performance of the DC-EDF. In this

research, we investigate and demonstrate the characterization of pulse operation in DC-EDF.

## **1.2 Problem statement**

There has been intense work on the pulse operation in the conventional (C-) band, long wavelength (L-) band as well as in the 2  $\mu\text{m}$  region. Nevertheless, as increasing demands for bandwidth have now pushed the envelope into the short-wavelength (S-band) region, it is of interest to further expand this coverage into the S-band region.

## **1.3 Thesis objective**

The main objective of this study is to study the characteristic of pulse operation on depressed cladding erbium doped fiber laser. In order to achieve this, two major steps of work are propose

- To propose and demonstrate pulsed operation in depressed-cladding erbium doped fiber laser.
- To study the wavelength range tunability of Q-switched operation in the S-band region.

## **1.4 Thesis arrangement**

Before any experiments are started, a literature review and understanding of operating principles of the pulsed operation, CNT, S-Band and DC-EDF are undertaken. After the review is completed, the experiment of S-band amplification using DC-EDF is done. Chapter 2 in this dissertation highlights the theoretical aspect involved in this work, including the depressed cladding erbium doped fiber (DC-EDF) as the gain medium, and the fundamental properties of the work. Chapter 3 outlines the methodology to achieve the objective of the work which are pulsed operation in depressed-cladding erbium doped fiber laser and tunability of Q-switched operation in the S-band region. Chapter 4 provides the experimental work and results on the

demonstration of pulsed operation in depressed-cladding erbium doped fiber laser and the tunability of Q-switched operation such as the average output power, output spectrum, repetition rate and pulse width. Chapter 5 concludes the dissertation and suggests future works to enhance greater development regarding the research in future.

University of Malaya

## CHAPTER 2: LITERATURE REVIEW

### 2.1 Introduction

This chapter begins with an overview of fiber lasers history and developments. The theoretical background of the generation S-band fiber laser is then discussed in this chapter. Then the chapter focuses on the gain medium that have been used in this work which is Depressed Cladding Erbium Doped Fiber. The chapter also will be discussing on pulse operations specifically Q-switched, Fabry perot etalon filter and lastly the saturable absorber used in this work, carbon nanotube and its fabrication process.

### 2.2 Fiber laser developments

50 years ago, the first fiber laser has been demonstrated by E. Snitzer in a Neodymium doped fiber (Rose Mary, Choudhury, & Kar, 2014; Snitzer, 1961; Snitzer, Hoffman, & Crevier, 1963). Currently, fiber lasers have find innumerable applications in a variety of fields ranging from medical diagnostics, laser material processing, imaging, metrology, and scientific research. Interestingly, fiber optics has revolutionized laser technology; especially since at the inception of both these technologies, this was far from envisaged. With the manufacturing success in low-loss optical fibers complemented by the advent of high-brightness semiconductor diode lasers, communication systems based on optical fibers were realized with advancement in terms of speed and data transmission capacity over long distances. Extensive research exploring further application potential of optical fibers grew only after this. Development of low-loss rare earth doped fibers in the 1980s led to the first reports of fiber lasers emitting output powers of the order of a few megawatts (Rose Mary et al., 2014; Mears, Reekie, Poole, & Payne, 1985). Since then, fiber laser technology has grown exponentially with average power outputs close to kilowatt range (Eidam et al., 2010; Y. e. Jeong, Sahu, Payne, & Nilsson, 2004; Rose Mary et al., 2014). The special advantages of fiber lasers over conventional solid state lasers have also led to their rapid

commercialization. The advancement in the field of fiber lasers can be attributed to certain defining features that arise due to their waveguide geometry. In fiber lasers, light is tightly confined to a small cross-sectional area, allowing high intensities within the core. Long lengths of the fiber can be used to obtain high gain, while still maintaining a rugged and compact cavity configuration. This makes these lasers highly stable. Another advantage is their ease of use. The laser beam delivery becomes inherently simple due to the fiber based configuration. The availability of high power laser diodes has allowed optical pumping of the system. Integrated cavities and all-fiber formats have become possible with the advent of fiber-coupled components and fiber Bragg gratings (Erdogan, 1997; Rose Mary et al., 2014). The high surface area to volume ratio in optical fibers allows excellent heat dissipation, facilitating unprecedented power scaling capacity. The high intensities in the fiber cores are however accompanied by undesirable nonlinear phenomena which results in power limitation, fiber facet damage (Limpert, Roser, Schreiber, & Tunnermann, 2006; Rose Mary et al., 2014) and fiber fuse effects (Kashyap, 2013; Rose Mary et al., 2014). The strength of the nonlinear effects depends on the intensity in the fiber core, and the interaction length. Considerable research has been undertaken with a view of overcoming these limitations for the optimization of fiber laser architectures. Examples include double-clad fiber design, and rare earth doped photonic crystal fibers (Limpert et al., 2006; Rose Mary et al., 2014). The most common rare earth doped fiber lasers (Rose Mary et al., 2014; Samson, Carter, & Tankala, 2011) use Ytterbium (Yb) and Erbium (Er) dopants, with their operating wavelength around 1.03  $\mu\text{m}$  and 1.5  $\mu\text{m}$ , respectively. Ytterbium doped systems have become increasingly popular over their Nd: doped bulk laser counterpart, due to the added advantages of low thermal load and the absence of fluorescence quenching. In fiber lasers, ultrafast operation is typically achieved by having an appropriate saturable absorber (SA), or by dispersion management in the system. In the

latter case, Yb doped fiber lasers work in the normal dispersion regime and rely on nonlinear polarization evolution for self-starting mode-locking (Chong, Buckley, Renninger, & Wise, 2006; Chong, Renninger, & Wise, 2007; Rose Mary et al., 2014). Semiconductor Saturable Absorber Mirrors (SESAM) (U Keller, 2010; Rose Mary et al., 2014), popularly used for mode-locked operation in solid-state bulk lasers have also been used in fiber systems (Gomes, Orsila, Jouhti, & Okhotnikov, 2004; Rose Mary et al., 2014). However, the use of SESAMs is not preferred since the fiber laser cavity design deters from being compact and alignment-free. The emergence of carbon nanotubes (CNT) and graphene as novel SAs have resulted in a new phase to the development of ultrafast lasers, including fiber lasers (Rose Mary et al., 2014; Shinji Yamashita, 2012). CNT and graphene have a broad operation wavelength, picosecond recovery times, and small modulation depths, allowing relatively simple passive mode locking of fiber systems.

Fiber lasers are currently in use in a variety of application regimes. For micromachining, which predominantly used CO<sub>2</sub> lasers, fiber lasers emerged as a superior alternative with easy beam delivery and a robust setup. They are also less bulky and more convenient to use compared to CO<sub>2</sub> lasers, which use Helium gas in the system (Rose Mary et al., 2014; Moeller, 1969). Consequently, micromachining has evolved at a rapid pace over the years, from hole drilling (Kamlage, Bauer, Ostendorf, & Chichkov, 2003; Rose Mary et al., 2014) and surface re-structuring (Rose Mary et al., 2014; Schoonderbeek, Schuetz, Haupt, & Stute, 2010) to fabrication of sub-micron features with high precision. Lasers have been used for micromachining both absorptive and transparent materials (Gattass & Mazur, 2008; Rose Mary et al., 2014).

Laser micromachining in transparent dielectrics was first demonstrated in 1996 by Davis et al. (Davis, Miura, Sugimoto, & Hirao, 1996; Rose Mary et al., 2014). They

reported a permanent refractive index change within a bulk dielectric by tightly focusing femtosecond laser pulses within the material. The mechanisms of material modification has since been widely studied, and is attributed to the nonlinear excitation processes that occur as a result of the high intensities at the laser focus (Gattass & Mazur, 2008; Rose Mary et al., 2014; Schaffer, Brodeur, & Mazur, 2001; Taylor, Hnatovsky, & Simova, 2008). Modification in materials have been manifested in a number of forms including material ablation (Rose Mary et al., 2014; Stuart et al., 1996), bubble formation (Bellouard & Hongler, 2011; Rose Mary et al., 2014), voids (Glezer & Mazur, 1997; Rose Mary et al., 2014; Schaffer, Jamison, & Mazur, 2004), nano cracks (Rose Mary et al., 2014; Sudrie, Franco, Prade, & Mysyrowicz, 2001; Taylor et al., 2008) and refractive index change (R Mary et al., 2012; Rose Mary et al., 2014; Schaffer et al., 2004). The type of modification depends highly on the nature of the material, and the inscription laser parameters. This type of direct laser writing offers a number of advantages over conventional waveguide fabrication methods. It is a rapid process requiring no clean room facilities as needed for thin-film deposition techniques. The process can also be employed in a wide variety of materials including many glasses, crystals and ceramics that are transparent to the operating wavelength of the laser.

Basic laser schematic generally entails a gain medium to provide amplification and an optical cavity to trap the light, creating a positive feedback. Lasing occurs when the total gain in the cavity is larger than the total losses. In fiber lasers, the gain medium is an optical fiber and there are three types of laser cavities depending on the topology: linear, ring and random (Pinto & Lopez-Amo, 2013).

The multiple scattering of photons in the amplifying medium rises the effective optical path, resulting in lasing (Pinto & Lopez-Amo, 2013; Wiersma, 2008). By using the intrinsic disorder of an optical fiber, a random laser can be attained. The refractive

index of optical fibers has submicron scale inhomogeneities that are randomly distributed along the fiber. Through propagation, the light will be scattered by these inhomogeneities obeying the Rayleigh's law (Headley & Agrawal, 2005; Pinto & Lopez-Amo, 2013). Taking advantage of these Rayleigh scattering events as an active part in the laser, this is saying as a distributed/random mirror in the laser cavity, can lead to the development of the laser's performance in three distinct ways: using the distributed random mirrors together with physical reflectors (in conventional resonant cavity) to enhance laser performance (Figure 2.1 A); using distributed mirrors with only one reflector, thus reducing the need for two mirrors (Figure 2.1 B); or even by not using physical reflectors at all, having then an all-fiber totally random fiber laser (Figure 2.1 C).

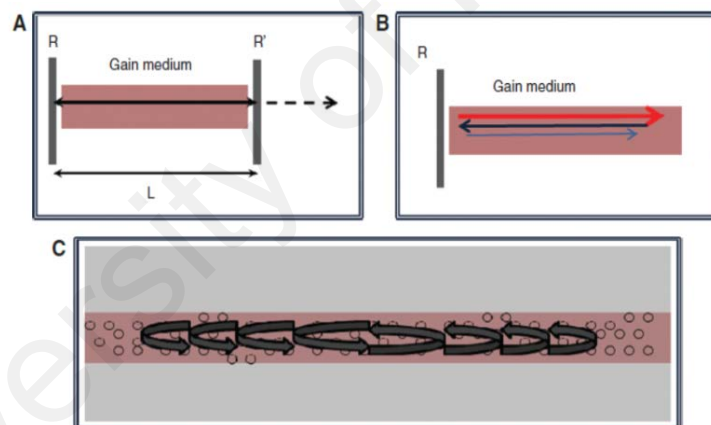


**Figure 2.1: Illustration of three different laser cavities: (A) conventional resonant cavity, (B) one reflector cavity and (C) random cavity (Pinto & Lopez-Amo, 2013)**

Laser cavities are designed using reflectors. There are varieties of reflectors that can be used in all-fiber lasers. A very common all-fiber laser reflector is the fiber loop mirror (FLM), due to its low sensitivity to environmental noise. These reflectors are designed forming a loop by fusion splicing the output ports of a directional coupler, resulting in low-loss and stable devices. The input light entering the optical coupler will be divided in two waves that travel with identical optical paths in opposite directions

and interfere when reentering the coupler. It was shown that the variation of reflectivity with wavelength and fiber birefringence of a perfect device (disregarding the losses of splice, fiber and optical coupler) can be adjusted from 0 to 100% by controlling the birefringence of the fiber loop (Mortimore, 1988; Pinto & Lopez-Amo, 2013). If the fiber loop mirror is constituted only by a fiber with no birefringence (or negligible birefringence, as in the case of common telecommunications single mode fiber) it will act as a perfect mirror: the light is reflected back into the input port while, due to the energy conservation, no light is transmitted to the output port. When there is birefringence in the loop, the two counter propagating waves will travel through the optical path with different velocities, due to the birefringence of the fiber. After propagating around the loop, the difference in the propagating wave's velocities will lead to a variable interference term in the output port (transmission and reflection). The wavelength spacing between two consecutive interference channels in the output spectrum is given by:

$$\Delta\lambda = \lambda^2/BL \quad 2.1$$

where B and L are the birefringence and length of the fiber, respectively. Fiber loop mirrors that exploit nonlinear phase shift of optical fibers are usually addressed as Sagnac interferometers (G. Agrawal, 2010; Mortimore, 1988; Pinto & Lopez-Amo, 2013). Another familiar type of laser reflector in all-fiber lasers is the Fabry-Perot interferometer (FPI), which consists of two mirrors of reflectance R1 and R2 separated by a cavity of length d. A light beam entering the cavity is reflected multiple times between the reflectors. Each beam has a fixed phase difference with respect to the preceding one; this phase difference corresponds to the extra path length travelled in the cavity. The FPI output signal is a periodic function with a period given by:

$$\Delta\lambda_{FPI} = \lambda^2/2nd \quad 2.2$$

There are also other interferometers that can be used as laser reflectors, such as Modal and Mach-Zehnder interferometers, but are not as commonly used. Another approach to design the fiber cavity is using gratings. Different kinds of gratings can be used, for example: fiber Bragg grating (FBG), which couples the forward propagating core mode to the backward propagating core mode; long-period fiber grating (LPG) that can couple the forward propagating core mode to one or a few of the forward propagating cladding modes; chirped fiber grating, that has a wider reflection spectrum and each wavelength component is reflected at different positions, which results in a delay time difference for different reflected wavelengths; tilted fiber grating can couple the forward propagating core mode to the backward propagating core mode and a backward propagating cladding mode; sampled fiber grating, can reflect several wavelength components with equal wavelength spacing; etc. Among all of them, the FBGs are the most widely used in laser cavities. In FBGs the Bragg wavelength, the wavelength at which the light that is reflected, is given by:

$$\lambda_{Bragg} = 2 \cdot n_{eff} \cdot \Lambda \quad 2.3$$

where  $n_{eff}$  is the effective refractive index of the fiber core and  $\Lambda$  is the grating period.

Ultrafast fiber lasers offer an unprecedented level of utility for many commercial and advanced scientific applications of ultrafast optics. The dissemination of ultrafast fiber lasers to the commercial and scientific realms are enabling by many advances in fiber laser technology as well as in ultrafast optical science during the last 20 years. For the future, we expect that fiber lasers will further feed novel exciting capabilities in the hyperspectral domain as well as in advanced frequency metrology. Potentially unprecedented power levels can be generated in the whole spectral range starting from the XUV all the way to the THz region. With new developments in fiber phase control techniques and fiber technology, such as improved ultra large core fiber amplifiers (L.

Dong et al., 2008; Fermann & Hartl, 2009), multicore fibers (Fermann & Hartl, 2009; Hartl, Marcinkevicius, McKay, Dong, & Fermann, 2009), and improved microstructured fibers, the benefits of fiber technology in the hyperspectral range are only expected to increase with time. Eventually, one can expect that as a result, the hyperspectral domain will not only lead to many advances in science and technology, but will also enable novel applications in the industrial domain. Further advances in high-peak-power lasers and plasma physics can be expected from the implementation of multicore fibers operating beyond the self-focusing limit as well as the implementation of coherent addition of individual fibers. With recent advancements in fiber frequency combs, optical clockworks based on fiber lasers appear to be feasible that could potentially be used in a new definition of world time standards. Other challenging applications that may come to fruition in the not too distant future are compact fiber-based electron accelerators, taking advantage of the fact that long-term absolute phase stability can be achieved with fiber lasers and novel electronic spectrometers (Coddington, Swann, & Newbury, 2008; Fermann & Hartl, 2009; Keilmann, Gohle, & Holzwarth, 2004).

### **2.3 S-band fiber laser**

There has been a growing interest in extending the existing bandwidths offered by C-band and L-band into Short wavelength also known as the S-band region. This was to overcome the limited bandwidths of DWDM systems at the time. The S-band operates between the wavelength regions of 1460 nm to 1520 nm, giving a window bandwidth of approximately 60 nm. This S-band bandwidth, when combined with the already available bandwidth of 70 nm from the C- and L-bands would give a total channel bandwidth of 130 nm, which could be able to cater to the increasing demand for capacity. There are several methods in achieving S-band amplification such as Fluoride-based Thulium-doped fiber amplifiers (TDFAs), Raman amplifiers and Depressed

Cladding-Erbium Doped Fiber (DC-EDF) amplifiers. However in this work, enhanced focus is given to DC-EDF since there are indicators that this method is efficient in terms of simplicity, reliability and cost.

Allowing S-band operation through Raman amplifier approach requires long dispersion compensating fiber (DCF) as the gain medium and high pump powers at each stage reported in (Z. Z. Sun et al., 2010). This proved to be relatively complex for the Raman amplifier method. In the same manner, Fluoride-based Thulium-doped fiber amplifiers approach had also exhibited some problems with regards to the S-band amplification. For example, (Chang et al., 2010) reported that it is difficult to use usual fusion splices to connect the active fluoride fiber with the silica fibers of the surrounding components due to low melting temperature of fluoride glass, which making it unworkable to combine TDFAs with conventional EDFAs to form an ultra-wide band EDFA.

Recently, another technique that was used to obtain S-band amplification is the use of a special type of EDF, known as DC-EDF. This type of fiber differs from the normal fibers by having two cladding layers instead of just one, with the outer cladding layer having a lower refraction index than the inner cladding layer. The advantage of this fiber is that it has a cut-off wavelength of 1525 nm, which is below the 1530 nm ASE peak in normal EDFs and thus prevents the lasing at this region.

#### **2.4 Depressed-cladding erbium doped fiber laser**

The Depressed Cladding Erbium Doped Fiber (DC-EDF) is a fiber that is designed to overcome the limitation of EDF in S-band amplification. To get amplification on S-band, the DC-EDF needs to be spooled with different spool diameter. The significant of doing this is to tune the cutoff wavelength of this fiber in order to filter out the C-band ASE thus getting amplification only in the S-band. However the spools cannot be too

small to prevent loss inside the DC-EDF fiber. The optimum spooled diameter which provides the highest ASE power in the S-band region is about 9cm. In order to obtain the S-band fiber laser by using the DC-EDF, the fundamental mode cutoff wavelength must be between the S-band and the long wavelength bands of the C- and L-band region. In particular the fundamental mode cut-off wavelength due to be S-band signal that remains in the core (M. A. Arbore et al., 2005) is preferably set near 1530 nm (Mark A. Arbore, 2005; Foroni et al., 2005). The fundamental mode cut-off can be determined by adjusting the cross section and refractive indices of core, depressed cladding and secondary cladding. The adjustment to the fundamental mode cut-off can also be made by adjusting the spooling diameter of the DC-EDF.

Depressed cladding is also known as W profile fiber due to its shape of index distribution that resembles the alphabet W. Dissimilar to the standard optical fiber (SMF-28), depressed cladding are surrounded by a secondary cladding. Within the depressed cladding fiber, the core, depressed cladding and secondary cladding all have a circular cross-section as show on the Figure 2.2.

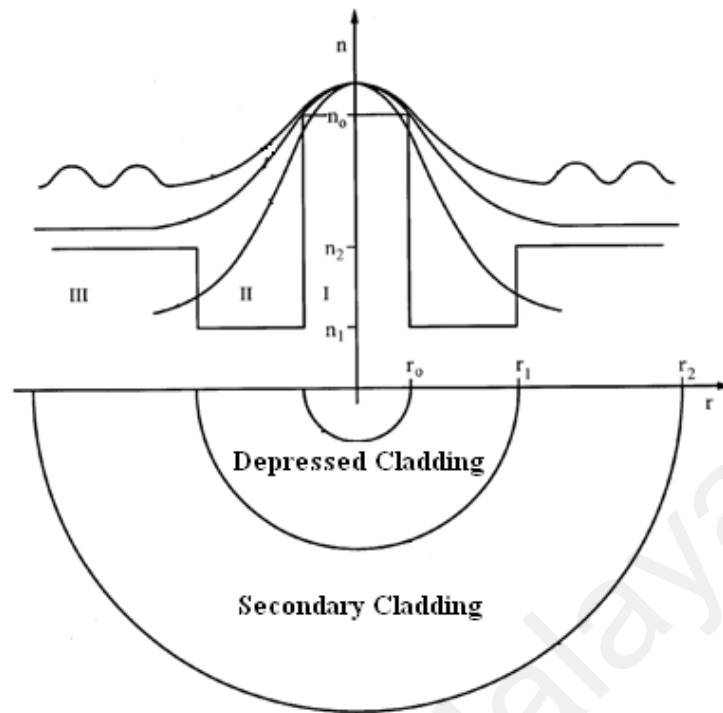


**Figure 2.2: Depressed cladding fibre cross-sectional view (M. Arbore & Keaton, 2003)**

At region I associated with core radius  $r$ , extends from  $0 \leq r \leq r_0$ , while the depressed cladding and secondary cladding radius occupy the regions of II, III which lies between  $0 \leq r \leq r_1$  and  $r \geq r_1$ . The core has an index refraction number  $n_0$ , while the depressed cladding has an index of refraction of  $n_1$  and the secondary cladding has an index of refraction of  $n_2$ .

Figure 2.3 shows the refractive-index profile of a single-mode fiber with depressed inner cladding. In addition to the propagations of guided modes in the core, discrete modes are also able to propagate in the outer cladding. Substantial power can be transferred from the core-guided mode to the outer cladding modes when the phase velocities of the modes are identical. Figure 2.3 illustrates the W-profile as obtained during normal manufacturing techniques. It is sufficient that the indices of the depressed cladding and secondary cladding average out to the values of  $n_1$  and  $n_2$  (M.A. Arbore, 2005).

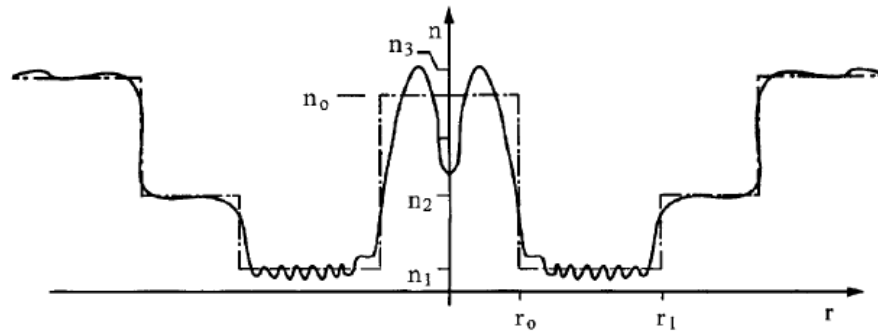


**Figure 2.3: W-Profile of Single Mode fiber (M.A. Arbore, 2005)**

The average index number of the core must be significantly higher than the index  $n_1$  of depressed cladding and the index  $n_2$  of secondary cladding. A selection of appropriate value for the indices  $n_0, n_1, n_2$  and radii  $r_0, r_1, r_2$  must be determined beforehand to have the desired fundamental cut-off wavelength.

## 2.5 Pulse operation

Some applications of lasers depend on a beam whose output power is constant over time. Such a laser is known as continuous wave (CW). For CW operation it is required for the population inversion of the gain medium to be continually replenished by a steady pump source. In some lasing media it is impossible. In some other lasers it would require pumping the laser at a very high continuous power level which would be impractical or destroy the laser by producing excessive heat. Such lasers cannot be run in CW mode. Pulsed operation of lasers refers to any laser not classified as continuous wave, so that the optical power appears in pulses of some duration at some repetition rate. In other cases the application requires the production of pulses having as large an energy as possible. Since the pulse energy is equal to the average power divided by the repetition rate, this goal can sometimes be satisfied by lowering the rate of pulses so that more energy can be built up in between pulses. (Popa et al., 2011; Popa et al., 2010).

There has been intense work on the pulse operation in the conventional (C-) band (Kasim et al., 2014; F. D. Muhammad, Zulkifli, & Ahmad, 2014; Zhao et al., 2014), long wavelength (L-) band (B. Dong, J. H. Hu, C. Y. Liaw, J. Z. Hao, & C. Y. Yu, 2011; R. Zhou et al., 2014) as well as in the 2  $\mu\text{m}$  region (J. F. Li et al., 2014; L. Wang et al., 2014). Nevertheless, as increasing demands for bandwidth have now pushed the envelope into the short-wavelength (S-band) region, it is of interest to further expand this coverage into the S-band region. In this research, DC-EDF is chosen to accomplish S-band fiber laser because of their ability to provide and maintain high level of inversion along the fiber.

### **2.5.1 Q-switched**

Compact and stable Q-switched fiber lasers have found interesting usage in the fields of laser processing, environmental sensing, medicine, range finding, optical communications, reflectometry, imaging, remote sensing, fiber sensing, manufacturing, and material processing (H. Ahmad, Zulkifli, Muhammad, Zulkifli, & Harun, 2013; Garnov, Konov, Kononenko, Pashinin, & Sinyavsky, 2004; Kracht & Brinkmann, 2004; Nikolaev, Pozhar, & Dzyubenko, 2006; H Shangguan, Casperson, & Prah, 1996; HanQun Shangguan, Casperson, Shearin, Gregory, & Prah, 1996; Siniaeva et al., 2009; Watanabe et al., 1991) due to their ability to yield high energy pulsed lasers. Generally, Q-switched fiber lasers can be achieved either through active or passive means. Of particular interest are passively Q-switched fiber lasers, which have a relatively simple configuration. Although earlier approaches use semiconductor saturable absorber mirrors (SESAMs) for realizing the passively Q-switched fiber lasers (Kivistö et al., 2008; Paschotta et al., 1999; Spühler et al., 1999), recently however, a far more simpler approach has been demonstrated, using carbon nanotubes (CNTs) (F. Ahmad et al., 2014; Ahmed et al., 2014; B. Dong, Hao, Hu, & Liaw, 2011; B. Dong, J. Hu, C.-Y. Liaw, J. Hao, & C. Yu, 2011; H. Jeong et al., 2014; Jung et al., 2012; Yu et al., 2014;

D.-P. Zhou, Wei, Dong, & Liu, 2010) and lately multiple layers of graphene (H. Ahmad, Zulkifli, Muhammad, et al., 2012; Cao, Wang, Luo, Luo, & Xu, 2012; Popa et al., 2011) to act as saturable absorbers (SA). Although graphene is a better candidate for SA applications due to its ultra-broad saturation range, covering the visible to mid-Infrared (IR) regions, as well as being wavelength independent, CNTs still has a high potential as a SA in fiber laser applications. This is because its ease of fabrication, requiring only deposition in a host material (usually available commercially) with a generally stable output in the Q-switched region.

Even though multiwavelength Q-switched lasers have been reported in the scientific literature, most of them have not managed to be extended into the S-band region. For example, the multi-wavelength Q-switched erbium doped fiber laser demonstrated by Bo Dong et al. (D.-P. Zhou, Wei, & Liu, 2012) only covers the wavelength lasing range of 1560-1563 nm that is in the C-band region. Moreover, the applications for Q-switched fiber lasers operating in the S-band region would be of great importance, such as described in (F. D. Muhammad et al., 2014).

In regards of the growing investigation on the wavelength tunability of a Q-switched fiber laser which has been widely demonstrated by the researchers (H. Ahmad et al., 2013; Cao et al., 2012; Bo Dong, Junhao Hu, et al., 2011; Han et al., 2014; Popa et al., 2011), study of the tunability performance of the Q-switched fiber laser in the S-band region also possess the similar significance. Reported work from reference (Popa et al., 2011) and (Han et al., 2014) demonstrate a wideband-tunable Q-switched fiber laser by using a tunable filter as the tuning mechanism, giving a tuning range of 33 nm (C-band) and 46 nm (C-band) respectively. A wider band tunability covering a wavelength range of about 50 nm (C- band) has been achieved in the proposed system of reference (Cao et al., 2012), which is also demonstrated using the tunable filter as the tuning mechanism.

On the other hand, a different approach for realizing the laser tunability has been reported in reference (Bo Dong, Junhao Hu, et al., 2011), which employs a variable optical attenuator (VOA) in the laser cavity to tune the gain spectrum. The tuning range obtained by this method is about 64 nm (C- and L- band). There also has been a report of using a tunable fiber Bragg gratings (TFBG) which is specially designed to enable the wavelength tuning (H. Ahmad et al., 2013), such that it could be extended or compressed. The tuning range of the TFBG however is quite limited due to the extension and compression limit of the TFBG, thereby providing a limited tuning range of only 10 nm.

In this work, a wideband tunable CNT-based Q-Switched fiber laser operating in the S-band region using a tunable Fabry-Perot etalon filter as the wavelength tuning and filtering mechanism is proposed and demonstrated. The system uses a 15 m long depressed-cladding erbium doped fiber (EDF) as the gain medium, while a thin CNT film is sandwiched between two connectors to function as the SA for the generation of the desired Q-switched pulses. The tuning range of the laser output carrying the Q-switching pulses covers a wide wavelength range of 47 nm, which spans from 1479 nm to 1526 nm. In addition, the lasing and Q-switching thresholds have a respective value of ~36 mW and ~65 mW. A repetition rate of 24.4 kHz is obtained at the maximum pump power of 100 mW at the wavelength of 1498 nm, together with a pulse width and pulse energy of 1.2  $\mu$ s and 26.1 nJ respectively.

The significance of this work is that a wideband tunable Q-switched pulse has been realized in a band different from the ordinary C-band region, which is the S-band region, by using the Fabry-Perot etalon filter as the wavelength tuning mechanism. Previously, tunable Q-switched fiber laser in the S-band region has been demonstrated by Muhammad et al. in (F. D. Muhammad et al., 2014), however with different tuning

mechanism, and smaller tuning range of about only 10 nm. This is the first time, to the knowledge of the authors, that a wideband tunable Q-switched pulse has been passively generated using CNT based SAs in the S-band region, with the tunability enabled by the tunable Fabry-Perot etalon filter. The use of Fabry-Perot etalon filter as the tuning mechanism in achieving tunable Q-switched fiber laser in this work proves that even with the incorporation of the filter in the cavity, the Q-switched pulse operation can still be conserved, though the use of the filter itself could not be justified novelty.

## 2.6 Fabry-Perot etalon filter

An optical filter is used to select the operating wavelength of the system. In this work, Fabry-Perot etalon filter is used as the filtering mechanism. Figure 2.4 shows the Fabry-Perot etalon filter from Micron Optics. The high optical resolution of the device is maintained, but with a few significant properties. It is important to ensure that the optical filter has fiber attached to both sides of the cavity. The etalon guides the light with each bounce between the mirrors and the device is equipped with a high resolution mechanical movement device. This filter is a piezoelectric transducer (PZT) used to position the mirrors which constitute the cavity. The wavelength can be selected by applying voltage to the PZT, thus allowing tuning over a wide spectral range.

The filter operates using two parallel reflecting surfaces separated by a distance of  $d$  from each other. The reflecting surface allows multiple and successive reflections of light which interferes constructively and destructively to produce an interference fringe output. The interference peaks depend on the distance  $d$  and the angle of the mirror relative to the incident light,  $\theta$  (Vaughan, 1989).

$$n\lambda = d \sin \theta \quad 2.4$$

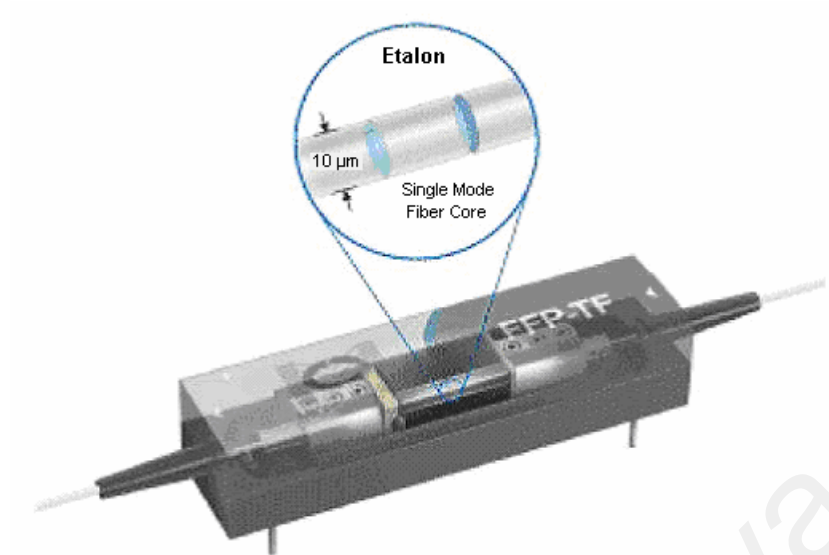


**Figure 2.4: Fabry-Perot etalon filter from Micron Optics**

Narrowband filters based on Fabry-Perot interferometers (FPI) are typically used to select the operating wavelength of the system. Fabry-Perot interferometer(FPI) sometimes called the Fabry-Perot etalon, consist of two mirrors of reflectance  $R_1$  and  $R_2$  separated by cavity of length  $L$  as in Figure 2.5

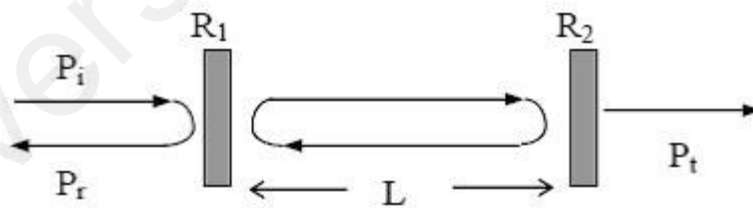


**Figure 2.5: Fabry-Perot interferometer, with  $P_i$ ,  $P_r$ , and  $P_t$  the incident, reflected, and transmitted optical power, respectively (Yin & Ruffin, 2002).**

## 2.7 Carbon nanotube

In the early 90s, Sumio Iijima have successfully become the pioneer in discovering CNTs (Iijima, 1991; Martinez & Yamashita, 2011). Since then, CNTs have become a prominent material for scientific and technological discipline which includes chemistry,

biology and electronics (Martinez & Yamashita, 2011; Nanotubes, 2001). The remarkable optical properties of CNTs have caused various theoretical and experimental studies have been reported in the late 90s (Kataura et al., 1999; Margulis & Sizikova, 1998; Martinez & Yamashita, 2011). Respectively, the potential applications of CNTs have been capturing higher attention from the photonics research community. CNTs exhibit an exceptionally high third-order optical nonlinearity and nonlinear saturable absorption with ultrafast recovery time and broad bandwidth operation. (Martinez & Yamashita, 2011).

CNTs are structures that belong to the fullerene family that are formed from a honeycomb sheet of  $sp^2$  bonded carbon atoms rolled seamlessly into itself to form a cylinder. Single-walled CNTs are approximately one-dimensional (1D) materials with a diameter that covers from 1 nm to 3 nm, and a length that ranges from 100 nanometers to centimetres. The electronic properties of single-walled CNTs are driven by a single criterion named chiral vector, which specifies the orientation of the tube axes with respect to the orientation of the honeycomb. Depending on this parameter, single-walled CNTs may behave as semiconductors or as metals. Those CNTs that behave as semiconductors exhibit a direct electronic bandgap which is directly proportional to the diameter of the nanotube. The optical absorption of CNT is determined by their electronic bandgap and broadband operation is a result of a large distribution of diameters formed during the CNTs fabrication (Kataura et al., 1999; Martinez & Yamashita, 2011). The discovery of the CNTs specialization has now spread to the use of CNTs in saturable absorption applications. Previous to that work, Margulis and Sizikova had estimated theoretically that CNT presents a very high third-order susceptibility  $X^3$  in the order of  $10^{-8} m^2/W$ . Third-order susceptibility is responsible for processes such as third harmonic generation (THG), optical Kerr effect, self-focusing and phase conjugation (Margulis & Sizikova, 1998; Martinez & Yamashita, 2011). Optical

communications and information technology that performs optical functions such as optical switching, routing and conversion required materials with high nonlinearity combined with fast response time which makes CNTs more valuable to be used in fibre lasers and nonlinear photonics devices. (Martinez & Yamashita, 2011).

Besides application mentioned above, CNTs have also found several other applications in photonics such as photodetectors, photovoltaic and nanometer-scale light devices (Avouris, Freitag, & Perebeinos, 2008). These applications rely on the properties of a single CNT and their potential applications in field-effect-transistor (CNT-FET) distributions. Such CNT-FETs not only have great potential towards the development of future optoelectronic applications, but also contribute an excellent platform to study optical phenomena in one-dimension. Nevertheless, the main purpose in this chapter applies in the CNT applications in the areas of optical communications and fiber lasers. Those applications are based on the CNTs nonlinear optical absorption which is useful for noise suppression and passive mode-locked lasing (Set, Yaguchi, Tanaka, & Jablonski, 2004) and their high nonlinearity which has a great potential towards the implementation of optical switches (Chen et al., 2002; Liu et al., 1999). These applications depend on using their combined optical properties and large number of CNTs. During their bulk fabrication, a large number of single-walled CNT with different tube diameters and electrical properties are generated. For most applications, the shortage of ability to fully influence the diameter and chiral vector of the CNTs during fabrication is a disadvantage. For optical fiber devices on the contrary, it is auspicious that the current fabrication processes produces a distribution of single-wall CNTs with different diameters, some behaving as a semiconductor and some as metals. The role of the semiconducting CNT is to sustain the saturable optical absorption, which is proportional to the diameter of each individual CNT. The wide distribution of CNT's

diameters provides broadband operation and the metallic CNTs also act as a crucial role towards decreasing the recovery time.

In the late 1990s, Margulis et al. reported the first theoretical study on the very high third order nonlinearity of CNT and Kataura et al. reported for the first time nonlinear optical properties of single-wall CNT, these are among the original interest to apply CNTs in photonics applications. The optical properties of CNTs are related closely to their structural and electronic properties and are fully governed by one parameter, its chiral vector, which define how the carbon-atom honeycomb is coordinated with respect to the CNT axis. Rely upon this parameter, CNTs may behave as a metal or a direct band-gap semiconductor (Martinez & Yamashita, 2011).

The electronic properties of a CNT are determined by its chiral vector. This vector describes how the graphene sheet is rolled when forming the nanotube. The chiral vector,  $C_h$  is expressed by two real space unit vectors  $a_1$  and  $a_2$  and two integers  $n$  and  $m$  as shown in equation :

$$C_h = n\bar{a}_1 + m\bar{a}_2 \quad 2.5$$

Graphene is a semimetal, when the single layer is rolled to form a tube an extra level of confinement into a quasi-1D structure is added. CNTs behave as metals if the subtraction of the integer values  $n$  and  $m$  is an integer multiple of 3 ( $n-m=3k$ ) otherwise it is a semiconductor ( $n-m \neq 3$ ). Hence, statistically it can be concluded that 2/3 of CNTs will be semiconductors, while 1/3 will be metallic CNTs. Saturable absorption is a result of the excitonic absorption in semiconductor nanotubes (Martinez & Yamashita, 2011; Saito, Fujita, Dresselhaus, & Dresselhaus, 1992).

### **2.7.1 Fabrication of CNT-based photonics devices**

Since 2003, certain laser methods and configurations in which to integrate the CNTs into the fiber have been recognized, each to suit different specifications. Initial devices were fabricated by spraying a solution of CNT in a substrate, mirror or fiber ferrule (Martinez & Yamashita, 2011; Set et al., 2004; S Yamashita et al., 2004) or by direct growth of the CNT in a substrate using chemical vapor deposition (CVD) (Song, Yamashita, Goh, & Set, 2007). In order to spray the CNTs, they are first independently dispersed into a solvent, such as Dimethylformamide (DMF) solvent by ultrasonification. This is significant in order to separate individual CNTs and breaking of bundles of CNT that are formed due to van der Waal forces. Once efficient dispersion is obtained the solution is subjected to configuration so the remaining agglomerated CNTs can be separated and discarded. While the spray technique is suitable to fabricate CNT-Saturable absorbers, the usage of CNT in order to coat the fiber is very high. During 2007, a method using an optical deposition technique CNT have been developed by Kashiwagi et al. and Nicholson et al. which the CNT could be deposited efficiently only in the core area of the fiber, reducing the CNT solution usage dramatically (Kashiwagi, Yamashita, & Set, 2007; Martinez & Yamashita, 2011; Nicholson, Windeler, & DiGiovanni, 2007).

### **2.7.2 Saturable Absorption**

Previously, the process for the bulk fabrication of CNTs do not allow complete control over the chirality and diameter of the fabricated CNTs. Instead, a combination of metal and semiconductor CNTs and multi-wall CNTs are produced during the fabrication. Nevertheless, researchers are now able to separate CNTs according to their chiral vector through post-fabrication. Hence, the ability to control the mean diameter and diameter distribution through the fabrication, purification and separation processes

is likely to further extend the applications of CNTs in photonics (Martinez & Yamashita, 2011).

The ultrafast response time of CNTs is based on bundle and entanglement of semiconducting and metallic CNTs because electrons which are excited by photons in semiconducting CNTs tunnel and couple to metallic CNTs, resulting in ultrafast recovery time of semiconducting CNTs. The combination of fast and slow processes within the CNT distribution, allows CNT to be very efficient saturable absorber both to self-start the mode locking operation and to produce ultrashort pulses. Plus, the inability to fully control the diameter of the CNTs during the growth is beneficial for the implementation of fiber laser. The wide distribution of CNT diameters is responsible for the broadband operation of CNT-based saturable absorbers (Martinez & Yamashita, 2011).

The recent advances in nanotechnology have the potential to overcome many of the shortcomings of traditional semiconductor technology. Nanotubes show great promise for optical devices. Single-wall nanotubes (SWNTs) exhibit strong optical absorption, covering a broad spectral range from UV to near IR. (O'connell et al., 2002; Zheng et al., 2003) To a first approximation, their band gap varies inversely with diameter. (Kataura et al., 1999) This can, in principle, be fine-tuned by modifying the growth parameters. Isolated semiconducting SWNTs (s-SWNTs) and small SWNT bundles exhibit photoluminescence (PL) in the near-IR spectral range (Bachilo et al., 2002; O'connell et al., 2002; Tan et al., 2007) PL is strongly quenched as the bundle size increases, which increases the probability of having metallic SWNTs (m-SWNTs) near s-SWNTs (O'connell et al., 2002; Reich, Thomsen, & Robertson, 2005; Tan et al., 2008; Tan et al., 2007). The PL properties of SWNTs have been extensively investigated over the past few years, (Bachilo et al., 2002; Chou et al., 2005; Lebedkin, Hennrich,

Kiowski, & Kappes, 2008; Maultzsch et al., 2005; Plentz, Ribeiro, Jorio, Strano, & Pimenta, 2005; Tan et al., 2007; Feng Wang, Dukovic, Brus, & Heinz, 2005) and the excitonic nature of electronic transitions in SWNTs has been theoretically predicted (Lefebvre & Finnie, 2008; Maultzsch et al., 2005; Perebeinos, Tersoff, & Avouris, 2005) and experimentally proven (Maultzsch et al., 2005; Feng Wang et al., 2005).

Selection of nanotubes is very important for the optimum performance of SWNT-based SAs. The nonlinear optical absorption depends on the number of nanotubes in resonance with the incident light. As the transition energies of SWNTs inversely vary with diameter, (Kataura et al., 1999) saturable absorption at a particular wavelength depends on the SWNT-diameter distribution (Sakakibara, Tatsuura, Kataura, Tokumoto, & Achiba, 2003). The SWNT-diameter distribution can usually be controlled by varying the growth parameters (Kataura et al., 2000; Lebedkin et al., 2002; Rozhin et al., 2006).

Pulse lasers with spectral-tuning capability have widespread applications in spectroscopy, biomedical research, and telecommunications (Fermann, Galvanauskas, & Sucha, 2002). The inclusion of a broadband SA can offer tunability over a range of wavelengths, unlike SESAMs. Compared to SESAMs, SWNT-based SAs possess a much wider operating range (Kieu & Wise, 2009; Kivistö et al., 2009; Z. Sun et al., 2008; Frank Wang et al., 2008) due to the inherent inhomogeneity of diameter (band gap) in as-prepared SWNT samples. (Hasan et al., 2009) realize tunable fiber lasers using SWNT-polymer SAs by fabricating a 40  $\mu\text{m}$  thick SWNT-PC composite with a broad absorption band (300 nm) centered at 1.55 $\mu\text{m}$  (Frank Wang et al., 2008) using SWNTs of 1–1.3nm diameter, covering the S, C, L, and U bands, as shown in Figure 2.6 (G. P. Agrawal, 2005). Note that the operating bandwidth of SWNTs is not the limiting factor for tunability (Hasan et al., 2009). In principle, the setup could enable

tuning for other bands, such as S (1460-1530 nm) and L (1565–1624 nm), if gain fibers and tunable filters at these wavelength ranges were available (Hasan et al., 2009).

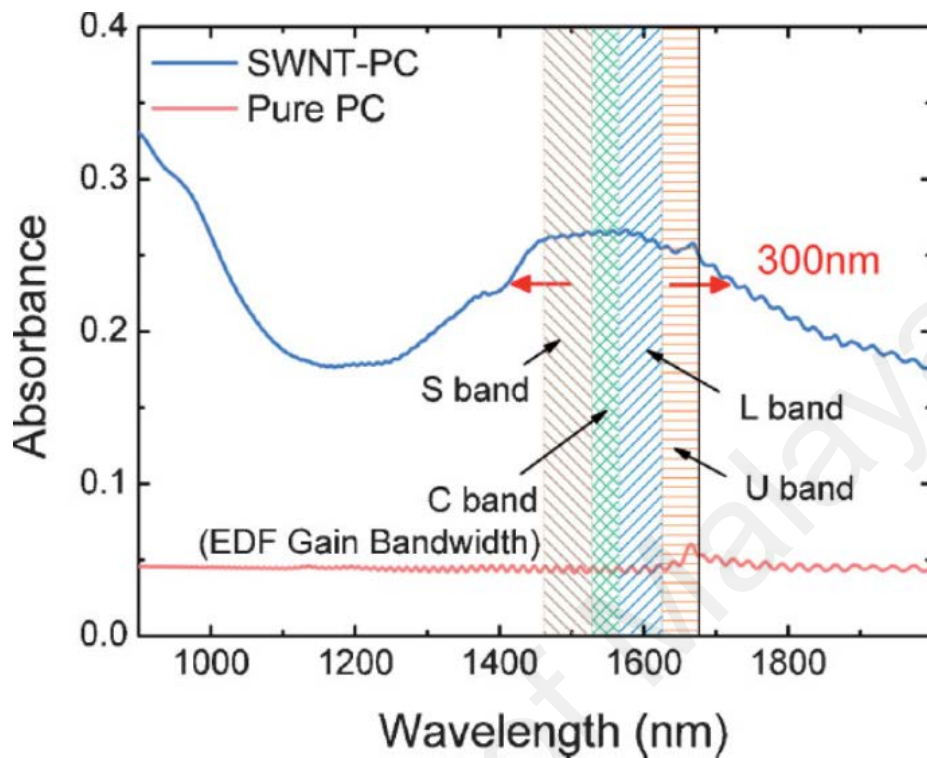


**Figure 2.6: Absorption spectra of a SWNT-PC composite and pure PC. The stripes show the telecommunication windows that can be potentially covered by this composite. S band: 1460-1530 nm, C band: 1530-1565 nm, L band: 1565-1625 nm and U band: 1625-1675 nm (Hasan et al., 2009)**

## CHAPTER 3: METHODOLOGY

### 3.1 Introduction

This chapter starts by introducing the optical devices used in the experiments which are laser diode, wavelength division multiplexing, optical isolator, coupler, fiber bragg grating and faraday rotator mirror. The principles and how it is used in the setup is briefly explained for each device. The chapter then continues with describing the methodology used in the experiment which includes the characterization of the pulse operation in depressed cladding erbium doped fiber laser, the tunibility wavelength of Q-switched operation in the S-band region and lastly the Single Longitudinal Mode Distributed Bragg Reflector Fiber Laser using depressed cladding erbium doped fiber. The experiment is well explained with detailed schematic diagram for each methodology.

### 3.2 Optical devices used in the experiments

#### 3.2.1 Laser Diode

Laser diodes are electrically pumped semiconductor lasers in which the gain is produced by an electrical current flowing through a p-n junction or (more frequently) a p-i-n structure. In such a heterostructure, electrons and holes can recombine, releasing the energy portions as photons. This process can be spontaneous, but can also be stimulated by incident photons, in effect leading to optical amplification, and with optical feedback in a laser resonator to laser oscillation (Keiser, 1999).

Most semiconductor lasers are based on laser diodes, but there are also some types of semiconductor lasers not requiring a diode structure and thus not belong to the category of diode lasers. In particular, there are quantum cascade lasers and optically pumped semiconductor lasers. The latter can be made of undoped semiconductor materials which cannot conduct significant electrical currents (Keiser, 1999). In this work, a TEC

laser diode has been used throughout the experiment as the pump laser source. Figure 3.1 shows the example of TEC laser diode.



**Figure 3.1: TEC laser diode**

### 3.2.2 Wavelength division multiplexing

Wavelength division multiplexing (WDM) is a kind of frequency division multiplexing where the optical signals with different wavelengths are combined, transmitted together, and separated again. It is mostly used for optical fiber communications to transmit data in several (or even many) channels with slightly different wavelengths. In this way, the transmission capacities of fiber-optic links can be increased strongly, so that most efficient use is made not only of the fibers themselves but also of the active components such as fiber amplifiers. Apart from telecom, wavelength division multiplexing is also used for interrogating multiple fiber-optic sensors within a single fiber (Ishio, Minowa, & Nosu, 1984).

Theoretically, the full data transmission capacity of a fiber could be exploited with a single data channel of very high data rate, corresponding to a very large channel

bandwidth. However, given the enormous available bandwidth (tens of terahertz) of the low-loss transmission window of silica single-mode fibers, this would lead to a data rate which is far higher than what can be handled by optoelectronic senders and receivers. Also, various types of dispersion in the transmission fiber would have very detrimental effects on such wide-bandwidth channels, so that the transmission distance would be strongly restricted. Wavelength division multiplexing solves these problems by keeping the transmission rates of each channel at reasonably low levels (e.g. 10 Gbit/s or 100 Gbit/s) and achieving a high total data rate by combining several or many channels (Keiser, 1999).

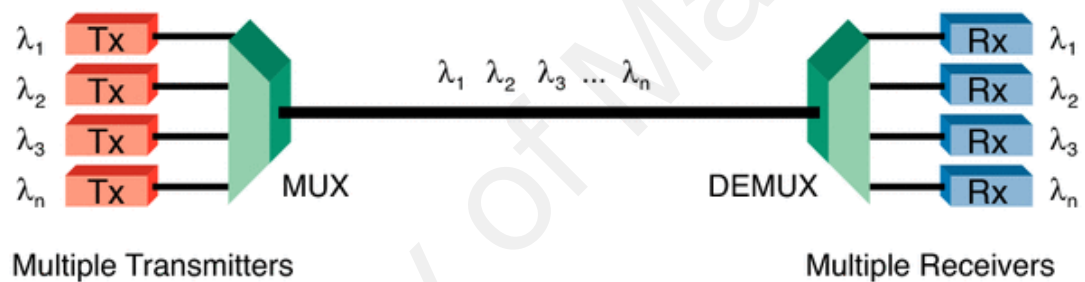


**Figure 3.2: wavelength division multiplexing**

### 3.2.3 Optical isolator

Optical isolators are one of the most important passive components in optical communication systems. The function of an optical isolator is to let a light beam pass through in one direction, that is, the forward direction only, like a one-way traffic. Optical isolators are used to prevent destabilizing feedback of light that causes undesirable effects such as frequency instability in laser sources and parasitic oscillation in optical amplifiers (Amemiya & Nakano, 2010).

Ordinary optical isolators available commercially make use of the Faraday effect to produce nonreciprocity. The Faraday effect is a magneto-optic phenomenon in which the polarization plane of light passing through a transparent substance is rotated in the

presence of a magnetic field parallel to the direction of light propagation. The Faraday effect occurs in many solids, liquids, and gases. The magnitude of the rotation depends on the strength of the magnetic field and the nature of the transmitting substance. Unlike in the optical activity (or natural activity), the direction of the rotation changes its sign for light propagating in reverse. For example, if a ray traverses the same path twice in opposite directions, the total rotation is double the rotation for a single passage. The Faraday effect is thus non-reciprocal (Amemiya & Nakano, 2010).

Figure 3.3 shows the schematic structure of an ordinary optical isolator. The isolator consists of three components, i.e., a Faraday rotator, an input polarizer, and an output polarizer. The Faraday rotator consists of a magnetic garnet crystal such as yttrium iron garnet and terbium gallium garnet placed in a cylindrical permanent magnet and rotates the polarization of passing light by  $45^\circ$ .

As illustrated in Figure 3.3, light traveling in the forward direction will pass through the input polarizer and become polarized in the vertical plane (indicated by  $P_i$ ). On passing through the Faraday rotator, the plane of polarization will be rotated  $45^\circ$  on axis. The output polarizer, which is aligned  $45^\circ$  relative to the input polarizer, will then let the light pass through. In contrast, light traveling in the reverse direction will pass through the output polarizer and become polarized by  $45^\circ$ . The light will then pass through the Faraday rotator and experience additional  $45^\circ$  of non-reciprocal rotation. The light is now polarized in the horizontal plane and will be rejected by the input polarizer, which allows light polarized in the vertical plane to pass through (Amemiya & Nakano, 2010).

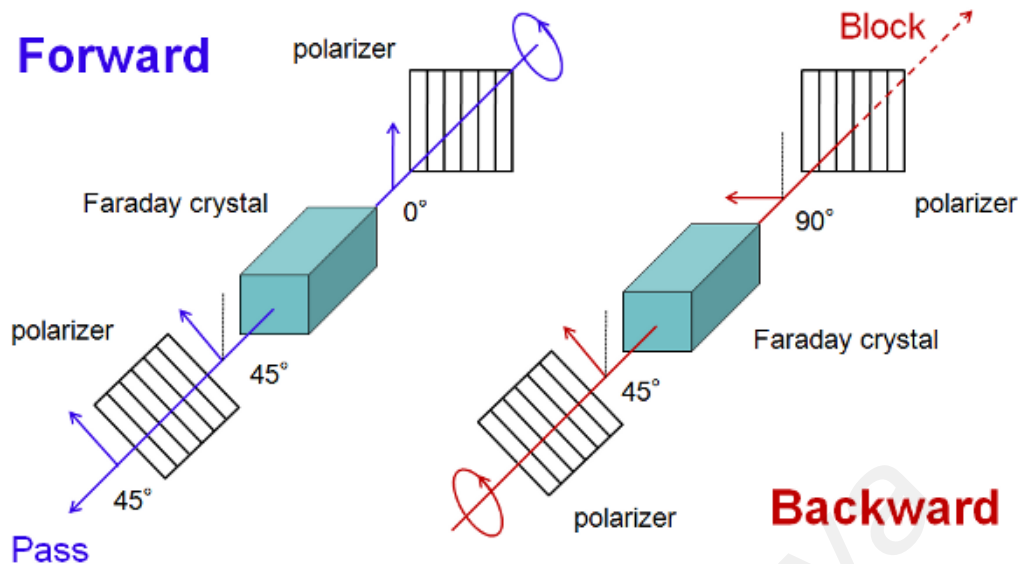


**Figure 3.3: Schematic structure of ordinary optical isolator (Amemiya & Nakano, 2010)**

### 3.2.4 Couplers

Fiber couplers belong to the basic components of many fiber-optic setups. FBT splitter, or FBT coupler, is an optical splitter that uses the Fused Biconic Taper (FBT) technique. The FBT technique is a well known industry technology for splitting optical power and/or splitting wavelengths. The fused fiber coupler is created through a process of fusing two bare fibers like an “X” and pulling the fused section to achieve the desired optical characteristics. FBT couplers are fused in tree structures to combine optical splitting effects to create power ratio output of  $1 \times N$  or  $2 \times N$ , where “N” is the number of desired outputs.

$1 \times 2$  FBT couplers are used to split light with minimal loss from one into two fibers or to merge light from two fibers into one.  $1 \times N$  tree FBT couplers and  $N \times N$  star FBT couplers are made with fuse cascade-connecting  $N-1$  pieces of  $1 \times 2$  and  $2 \times 2$  couplers respectively. Figure 3.4 shows a simple  $1 \times 2$  coupler with one input and two outputs.

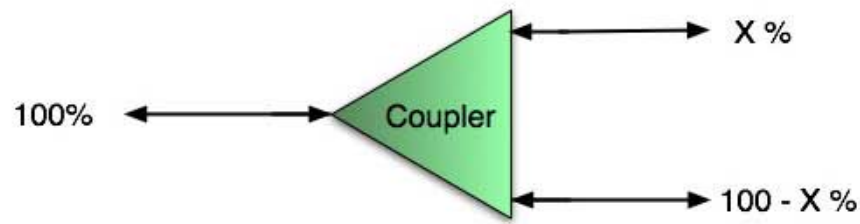


**Figure 3.4: A simple 1X2 coupler with one input and two outputs**

### 3.2.5 Fiber Bragg Gratings

A Fiber Bragg Grating (FBG) is a periodic perturbation of the refractive index along the fiber length which is formed by exposure of the core to an intense optical interference pattern. The formation of permanent gratings in an optical fiber was first demonstrated by Hill et al. in 1978 at the Canadian Communications Research Centre (CRC), Ottawa, Ont., Canada, (K. Hill, Fujii, Johnson, & Kawasaki, 1978; K. O. Hill & Meltz, 1997; Kawasaki, Hill, Johnson, & Fujii, 1978). They launched intense Argon-ion laser radiation into a germania-doped fiber and observed that after several minutes an increase in the reflected light intensity occurred which grew until almost all the light was reflected from the fiber. Spectral measurements, done indirectly by strain and temperature tuning of the fiber grating, confirmed that a very narrowband Bragg grating filter had been formed over the entire 1-m length of fiber. This achievement, subsequently called “Hill gratings,” was an outgrowth of research on the nonlinear properties of germania-doped silica fiber. It established an unknown photosensitivity of Germania fiber, which prompted other inquires, several years later, into the cause of the fiber photo-induced refractivity and its dependence on the wavelength of the light which was used to the form the gratings. Detailed studies (K. O. Hill & Meltz, 1997; Lam & Garside, 1981) showed that the grating strength increased as the square of the light

intensity, suggesting a two-photon process as the mechanism. In the original experiments, laser radiation at 488 nm was reflected from the fiber end producing a standing wave pattern that formed the grating. A single photon at one-half this wavelength, namely at 244 nm in the ultraviolet, proved to be far more effective. Meltz et al. (K. O. Hill & Meltz, 1997; Meltz, Morey, & Glenn, 1989) showed that this radiation could be used to form gratings that would reflect any wavelength by illuminating the fiber through the side of the cladding with two intersecting beams of UV light; now, the period of the interference maxima and the index change was set by the angle between the beams and the UV wavelength rather than by the visible radiation which was launched into the fiber core. Moreover, the grating formation was found to be orders-of-magnitude more efficient. At first, the observation of photo-induced refractivity in fibers was only a scientific curiosity, but over time it has become the basis for a technology that now has a broad and important role in optical communications and sensor systems (K. O. Hill & Meltz, 1997).

Research into the underlying mechanisms of fiber photosensitivity and its uses is on-going in many universities and industrial laboratories in Europe, North and South America, Asia, and Australia. Several hundred photosensitivity and fiber grating related articles have appeared in the scientific literature and in the proceedings of topical conferences, workshops, and symposia. FBG's are now commercially available and they have found key applications in routing, filtering, control, and amplification of optical signals in the next generation of high-capacity WDM telecommunication networks. (K. O. Hill & Meltz, 1997). Figure 3.5 shows an expanded View of an FBG.

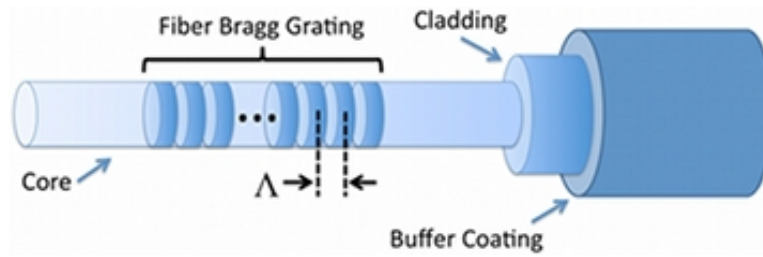


**Figure 3.5: An Expanded View of an FBG**

### 3.2.6 Faraday rotator mirror

A Faraday rotator is a magneto-optic device, where light is transmitted through a transparent medium which is exposed to a magnetic field. The magnetic field lines have approximately the same direction as the beam direction, or the opposite direction. If the light is linearly polarized in some direction, this polarization direction is continuously rotated during the passage through the medium. The total rotation angle  $\beta$  can be calculated as:

$$\beta = VBL \quad 3.1$$

where  $V$  is the Verdet constant of the material,  $B$  is the magnetic flux density (in the direction of propagation), and  $L$  is the length of the rotator medium. Note that the Verdet “constant” usually exhibits substantial wavelength dependence: it is smaller for longer wavelengths.

An important aspect is that the change of polarization direction is defined only by the magnetic field direction and the sign of the Verdet constant. If some linearly polarized beam is sent through a Faraday rotator and back again after reflection at a mirror, the polarization changes of the two passes add up, rather than canceling each other. This non-reciprocal behavior distinguishes Faraday rotators e.g. from arrangements of waveplates and polarizers. Concerning the physical origin of the polarization rotation, one may consider a linearly polarized beam as a superposition of two circularly

polarized beams. The magnetic field causes a difference in phase velocity between these circularly polarized components. The resulting relative phase shift corresponds to a change in the linear polarization direction.

A particularly important application is in Faraday isolators, as needed e.g. to protect lasers and amplifiers against back-reflected light. For that application, the rotation angle should be close to  $45^\circ$  in the spectral region of interest. A highly uniform polarization rotation is desirable to obtain a large attenuation for back-reflected light. A Faraday rotator in a ring laser resonator can be used to introduce round-trip losses which depend on the direction and thus enforce unidirectional operation. As only a very small loss difference is often sufficient, a Faraday rotator only provide a very small rotation angle may be sufficient. An additional half-waveplate may be used to compensate the polarization rotation for one beam direction. Figure 3.6 shows of a double-pass laser amplifier. The Faraday mirror on the right side ensures that the polarization state of light is not distorted after a double pass through the amplifier medium. A  $45^\circ$  the rotator combined with an end mirror forms a Faraday mirror. If a laser beam is send through some amplifier, then reflected at such a Faraday mirror and sent back through the amplifier, the returning beam has a polarization direction which is orthogonal to the input beam – even if the polarization state is not preserved within the amplifier. Therefore, a polarizer can reliably separate the counter propagating beams. This works better than using a Faraday isolator (with an output port for reflected light), an amplifier and an ordinary mirror.

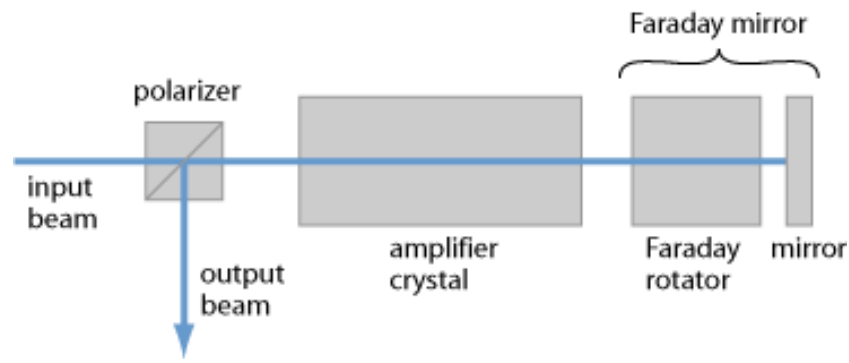


**Figure 3.6: Setup of a double-pass laser amplifier that includes the Faraday mirror.**

### **3.3 To characterize pulsed operation in depressed-cladding erbium doped fiber laser**

Figure 3.7 shows the experimental setup of the proposed Q-switched S-band fiber laser. The setup consists of a 15 m long depressed-cladding EDF, which has an absorption coefficient of approximately 6.2 dB/m at wavelength of 1530 nm, as well as absorption peaks of 7.6 dB/m at 1500 nm. To allow for operation in the desired region of 1500 nm, the depressed-cladding EDF is spooled with a diameter of about 9 cm so as to inhibit operation at wavelengths of more than 1530 nm. As this fiber provides a high-distributed loss for wavelengths longer than 1525 nm, the amplification in S-band region could be achieved (Chan et al., 2009). A 980-nm laser diode (LD) is used as the fiber laser pump source and is connected to the 980-nm port of a wavelength division multiplexer (WDM). The common output of the WDM is connected to the 15-m-long depressed-cladding EDF, which acts as the gain medium for the laser. The other end of the depressed-cladding EDF is connected to the input of an optical isolator to ensure unidirectional oscillations within the ring cavity. The output port of the isolator is connected to a 90:10 fused fiber coupler, which is used to extract a portion (10%) of the laser oscillating in the cavity for analysis. The remaining signal is channeled through the 90% port of the coupler where it will then propagate through the Carbon Nanotube

(CNT)-based Saturable Absorber (SA), whereby the CNT layer is sandwiched between two fibers connectors which are clasped using an FC/PC adaptor. The CNT has an operational wavelength of about 1.5  $\mu\text{m}$  and is in the form of thin film. The SA acts a passive Q-switching element. The output of the SA is connected to the 1550-nm port of the WDM, thereby completing the ring cavity. The laser output is analyzed by a Yokogawa AQ6317 optical spectrum analyzer (OSA) with a resolution of 0.02 nm, while the Q-switched pulse train characteristics are measured using a LeCroy 352A oscilloscope together with an Agilent 83440C photodetector.

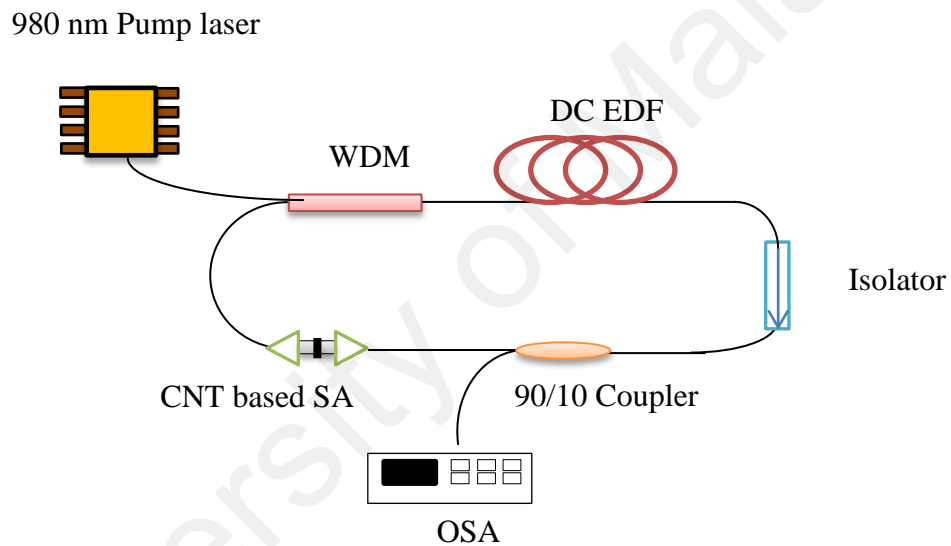


**Figure 3.7: Experimental setup of the proposed Q-switched S-band fiber laser**

### 3.4 To study the wavelength range tunability of Q-switched operation in the S-band region

To investigate the tunable Q-Switched fiber laser operating in the S-band region, a tunable Fabry-Perot etalon filter is inserted in the setup as the wavelength tuning and filtering mechanism. This Fabry-Perot is located between the CNT saturable absorber and 90/10 coupler. The setup is shown in figure 3.8. Figure 3.8 shows the experimental setup of the proposed tunable Q-switched S-band fiber laser using tunable Fabry-Perot etalon filter.

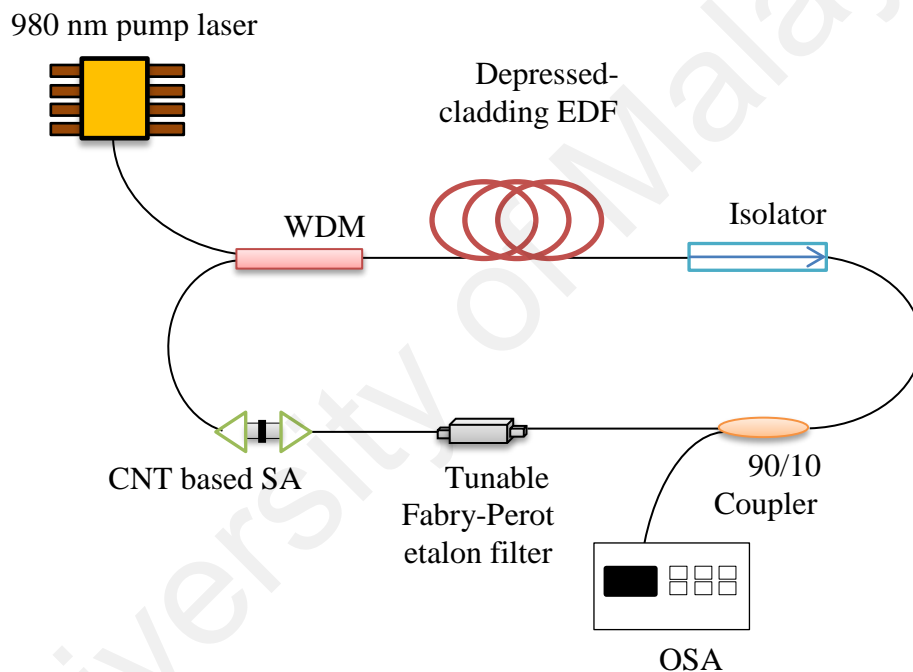


**Figure 3.8: Experimental setup of the proposed tunable Q-switched S-band fiber laser**

### 3.5 SLM Distributed Bragg Reflector Fiber Laser using DC-EDF

Figure 3.9 shows the experimental setup for the SLM DBR fiber laser. The DC-EDF absorption coefficients are approximately 6.2 dB/m at a wavelength of 1530 nm, as well as absorption peaks of 7.6 and 1.2 dB/m respectively at 980 and 1500 nm. To allow for operation in the desired region of 1500 nm, the DC-EDF is spooled with a diameter of about 9 cm so as to inhibit operation at wavelengths of more than 1530 nm. As this fiber provides a high-distributed loss for wavelengths longer than 1525 nm, the amplification in S-band region is thus achievable (H. Ahmad, Saat, & Harun, 2005). A 980 nm laser diode (LD) is used as the fiber laser pump source and is connected to the 980 nm port of a wavelength division multiplexer (WDM). The common output of the WDM is connected to the input port of the FBG, with central wavelength of 1506 nm and reflectivity of about 70%, which is part of the DBR laser cavity and acts as the ‘front mirror’. The FBG output is connected to a 15 m long DC-EDF, which acts as the gain medium for the laser. The other end of the DC-EDF is connected to a Faraday reflector mirror (FRM), which serves as the ‘back mirror’ for the linear cavity. The laser will then oscillate in the cavity formed by the FBG and FRM, and the filtered output is extracted through the WDM via the 1550 nm port. An optical spectrum analyzer (OSA) (AQ6317, YOKOGAWA, Japan) is used to analyze the generated spectrum output.

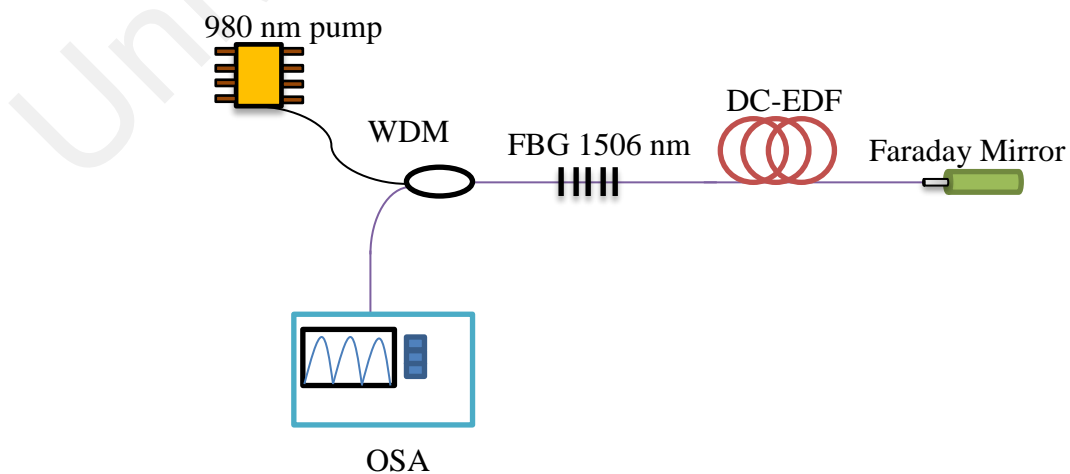


**Figure 3.9: Experimental setup for the SLM DBR fiber laser using DC-EDF**

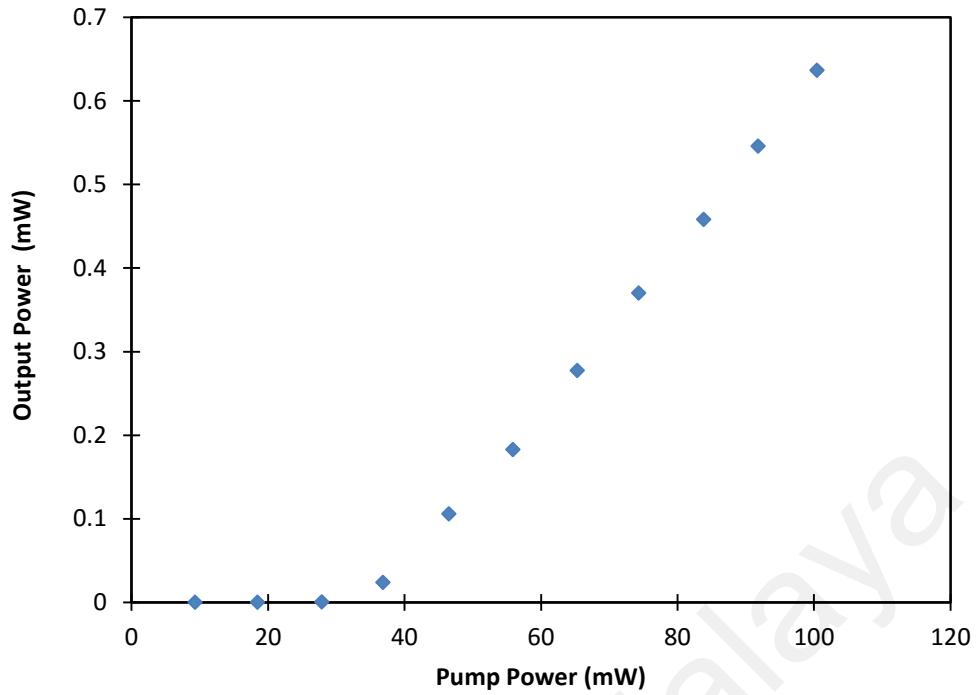
## CHAPTER 4: RESULTS AND DISCUSSION

### 4.1 Introduction

This chapter will focus on the findings that have been obtained during the study. The subtopics are divided by the types of experiments which are Q-switched S-band fiber laser, tunable Q-switched DC-EDF laser using CNT by Fabry-Perot etalon filter and SLM Distributed Bragg Reflector Fiber Laser using DC-EDF. The results are detail out by each section and been analyze based on the repetition rate, pulse width, spectrum and other aspects. In the last experiment, further verification of the SLM operation of the system is achieved by using the delayed self-heterodyned technique.

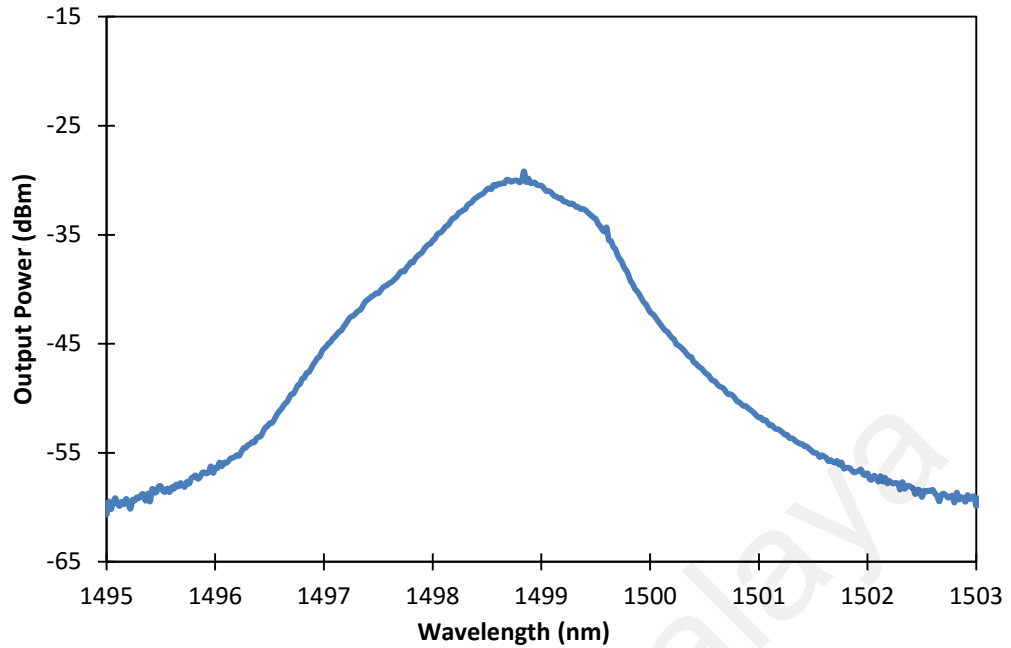
### 4.2 Q-Switched S-band Fiber laser

Figure 4.1 shows the average output power against the pump power of CNT-based Q-Switched S-band fiber laser. A linear relationship between the average output power and pump power is obtained, as shown in the figure, with a slope efficiency of 0.96%. The maximum average output power of ~0.64 mW is obtained at the highest pump power of ~100 mW. Higher average output power is expected to be achieved provided that the pump power is further increased above 100 mW. However, due to the limitation of the pump laser, the output power characteristics for the pump power exceeding 100 mW is not demonstrated. This proposed system has a lasing threshold of ~36 mW.



**Figure 4.1: Output power as a function of pump power**

Figure 4.2 shows the output spectrum of the proposed Q-switched S-band fiber laser taken from the OSA with a spectral resolution of 0.02 nm at pump power of 100.4 mW. As can be seen from the figure, the laser spectrum covering the wavelength range from approximately 1495 nm to 1503 nm at -55 dBm output power level. The peak wavelength of the spectrum is at about 1498.7 nm, having an output power of about -30 dBm. The 3 dB bandwidth of the output spectrum is 1.2 nm. The factors that probably contribute to the broad laser bandwidth obtained in this work are due to the multimode oscillations and also the emission of photons at long wavelength (X. L. Li, Xu, Wu, He, & Hao, 2011).



**Figure 4.2: Output spectrum of the proposed Q-switched S-band fiber laser**

The repetition rate and the pulse width of the generated Q-switched pulses at different pump powers are given in Figure 4.3. Q-switched operation only begins at a pump power of approximately 65 mW, with a repetition rate value of 8.2 kHz. Steadily increasing the pump power results in a similar response to the repetition rate, thus demonstrating that the repetition rate is dependent on the pump power (Zhou et al., 2010). At the highest pump power of approximately 100 mW, the highest repetition rate of 24.4 kHz is obtained. It is predicted that increasing the pump power above 100 mW can further increase the repetition rate value. On the other hand, the output pulse width of this proposed system decreases with the pump power. From a value of 3.8  $\mu$ s at the Q-switching threshold of 65 mW, the pulse width quickly reduces to about 1.2  $\mu$ s as the pump power is increased to its maximum value of  $\sim$ 100 mW. It can be deduced that both the repetition rate and pulse width vary with pump power, such that, the higher the pump power, the higher the repetition rate value. As in the case of pulse width, the higher the pump power, the narrower the pulse width value. In order to further improve the output performance of the pulse width, it would be necessary to have a saturable

absorber with a shorter recovery time since the pulse width in Q-switching mainly depends on time required to deplete the gain after the saturable absorber has been saturated (U. Keller et al., 1996; Popa et al., 2011; Svelto, 1998). Generally, the recovery time of a saturable absorber can be engineered through the fabrication process of the saturable absorber.

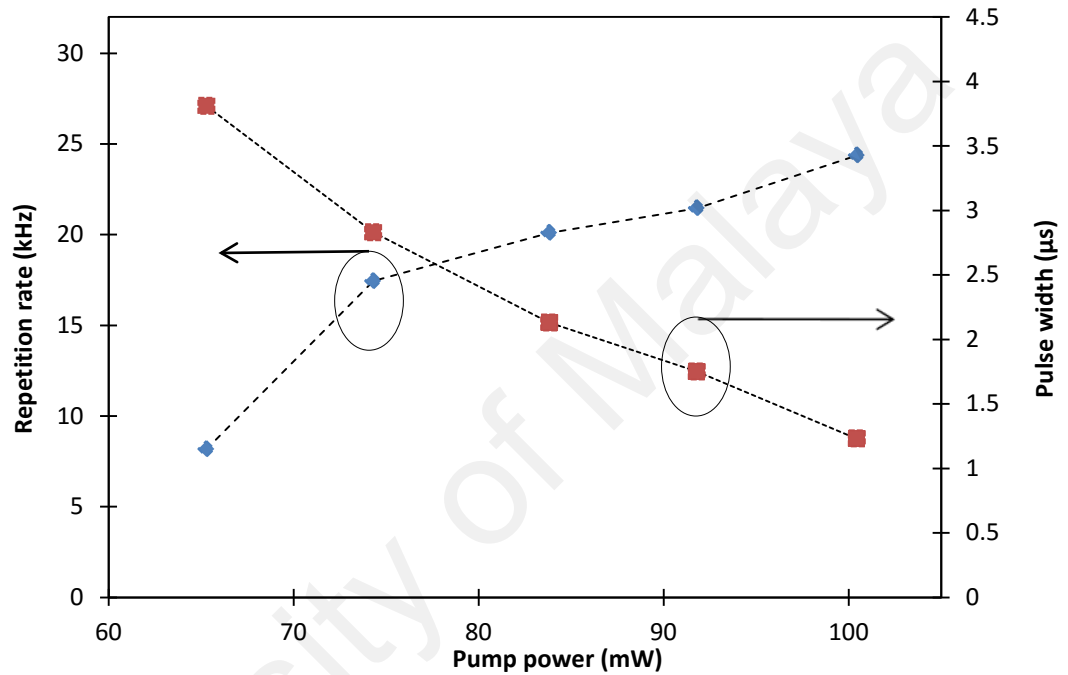


**Figure 4.3: Repetition rate and pulse width against pump power**

The output pulse train of this Q-switched S-band fiber laser is plotted in Figure 4.4, which is taken at the output wavelength of 1499 nm respectively. As can be seen from Figure 4.4, the repetition rate value is 25.9 kHz, corresponding to a time interval between the pulses of 38.6 µs. The pulse train is taken at the maximum pump power of ~100 mW.

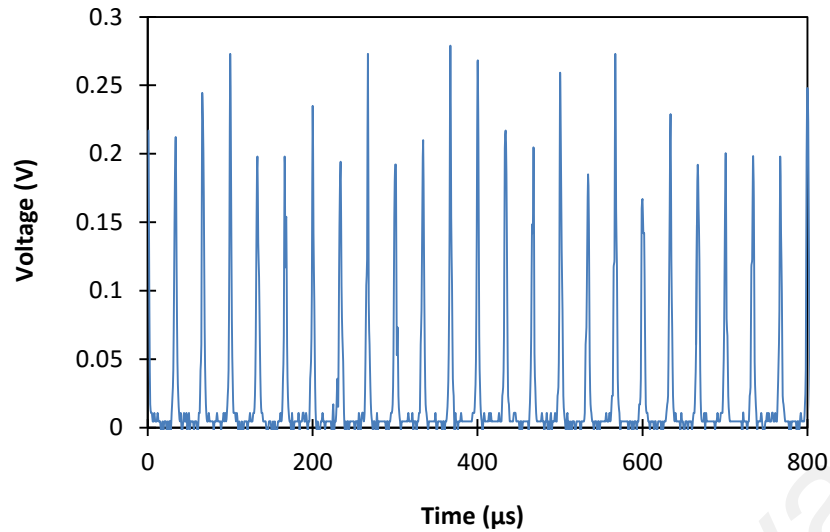


**Figure 4.4: Output pulse train at wavelength of 1499 nm with repetition rate value of 25.9 kHz**

#### **4.3 Tunable Q-switched DC-EDF laser using CNT by Fabry-Perot etalon filter**

The variation of the repetition rate at different wavelengths from 1479 nm to 1526 nm by tuning the Fabry-Perot filter with the pump power fixed at 100 mW is shown in Figure 4.5. From the figure, it can be seen that the repetition rate varies slightly across the wavelength. This could be attributed to the gain difference of the depressed-cladding EDF as well as the insertion loss of the filter that varies across the wavelength, and will consequently cause the change in the repetition rate at different wavelengths (J. L. Dong et al., 2011). The highest repetition rate achieved is 29.7 kHz at 1519 nm, whereas the lowest repetition rate measured is 15.0 kHz at 1489 nm. It is expected that a wider wavelength range with the Q-switching pulse operation could be attained by having a broader bandwidth of the ASE spectrum.

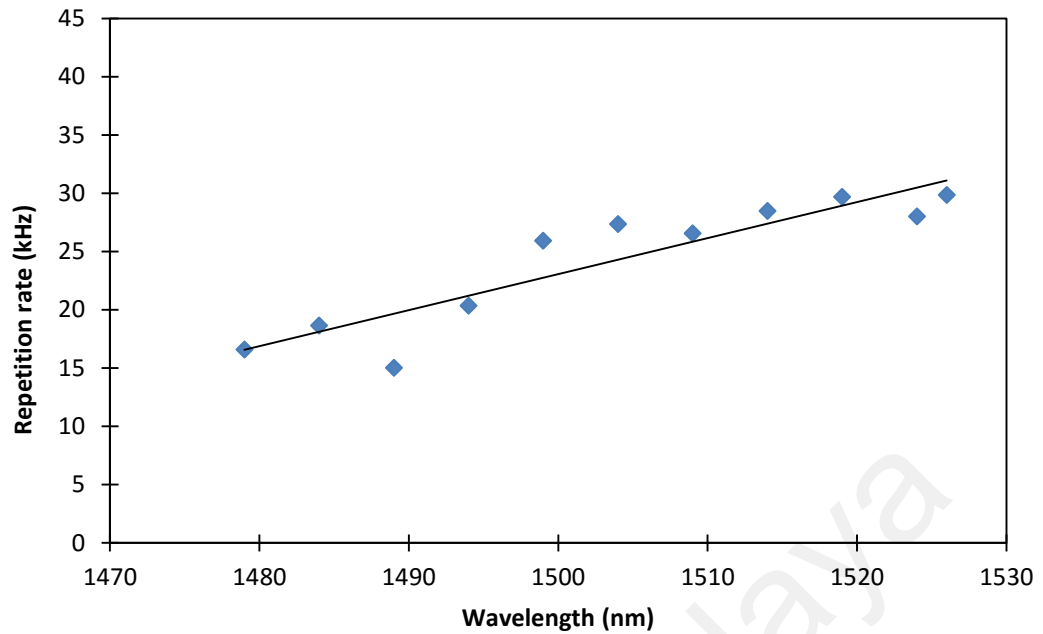
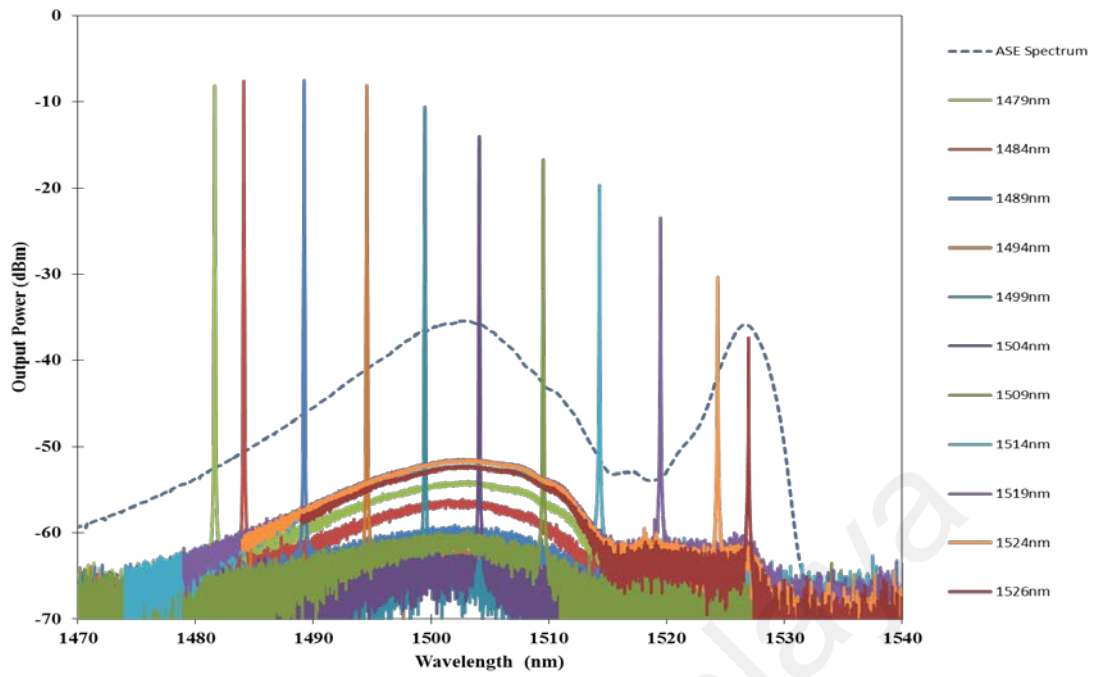
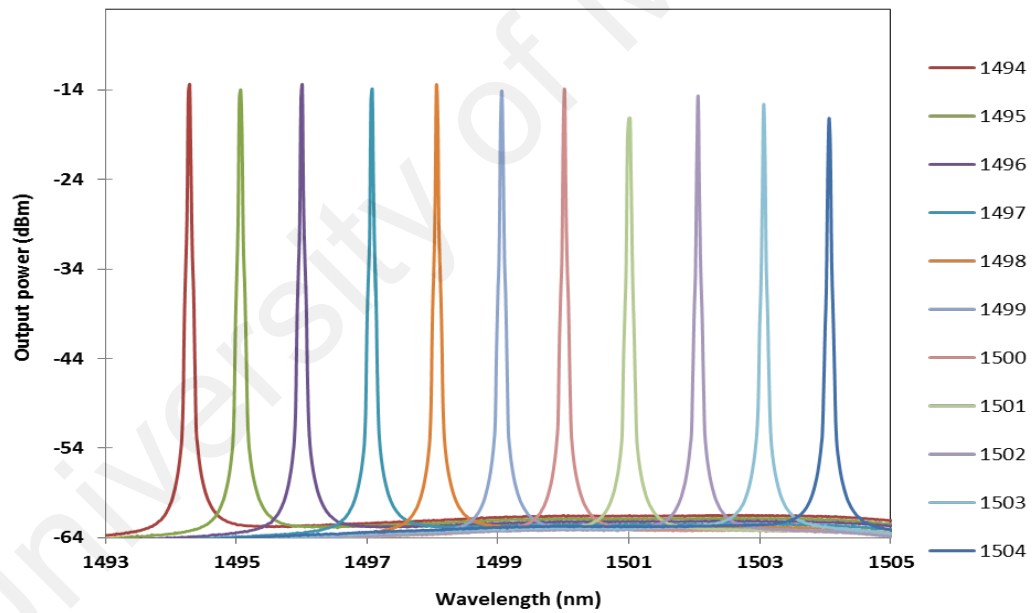


**Figure 4.5: Repetition rate against wavelength at pump power 100 mW**

Figure 4.6 (a) shows the output spectra of the tunable Q-switched S-band fiber laser for the 11 tuned wavelengths at the interval of 5 nm taken from the OSA at the pump power of ~100 mW. The tuning range of the laser output carrying the Q-switching pulses covers a wide wavelength range of 47 nm, which spans from 1479 nm to 1526 nm. However, due to the limitation of the amplified spontaneous emission (ASE) spectrum of the depressed-cladding EDF itself, as shown in the figure (presented by dashed line), the wavelength tuning of the laser output is also limited. This also explains the reason to the observed phenomenon of decreasing peak power of the output spectrum towards the longer wavelength. Figure 4.6 (b) shows the zoom in view of the output spectra taken at a wavelength interval of 1 nm. The tunable Fabry-Perot etalon filter can be tuned manually by adjusting the voltage supplied to the filter from the smallest scale of 0.1 V, the wavelength shift is dependent on the resolution of the applied voltage. By careful tuning the filter, a smaller wavelength shift of less than 0.5 nm could be attained.



(a)



(b)

**Figure 4.6: (a) Output spectra of the proposed system for 11 tuned wavelengths at an interval of 5 nm at pump power 100 mW**

**(b) Zoom in view of the output spectra at a wavelength interval of 1 nm**

The output pulse train of this tunable Q-switched S-band fiber laser is plotted in Figure 4.7 which is taken at the output wavelength of 1509 nm. As can be seen from Figure 4.7, the repetition rate value is 26.5 kHz, corresponding to a pulse interval of

37.7  $\mu\text{s}$ . The pulse train is taken at the maximum available pump power of  $\sim 100$  mW. As can be seen from the figure, the output pulse train as observed from the oscilloscope shows no partial mode-locking behaviour, as indicated by the evenly pulse spacing between the pulses. However, it can also be observed that the magnitude of the individual pulse is not uniform and unstable. This could be attributed by the high pump power when the pump power is increased to its maximum value, which causes the rise of the peak output power and consequently increases the spontaneous emission noise. This spontaneous emission noise is responsible for the perturbation and fluctuation of the output pulse, as described in Ref. (F. Ahmad et al., 2014). Similar phenomenon of this unstable pulse train has also been reported in Ref.(F. Ahmad et al., 2014).

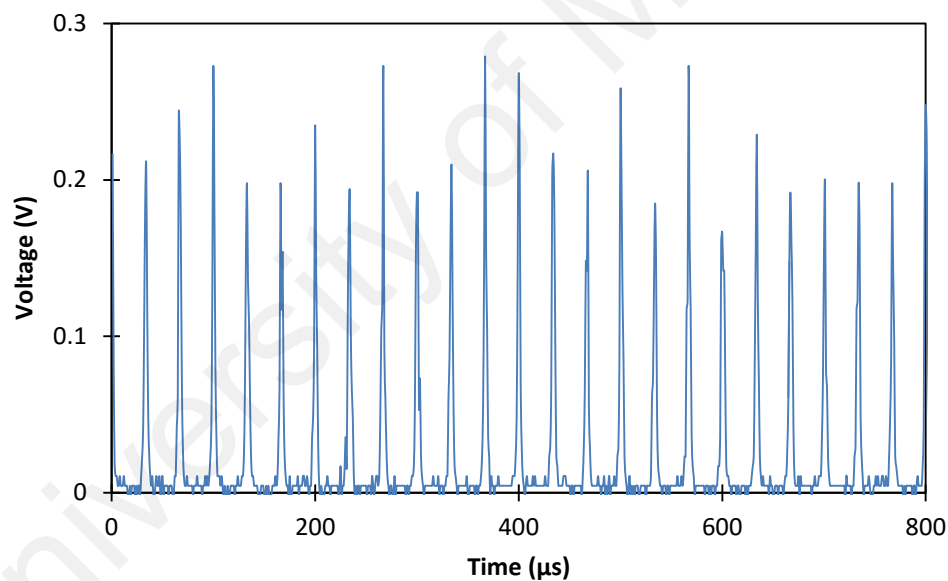
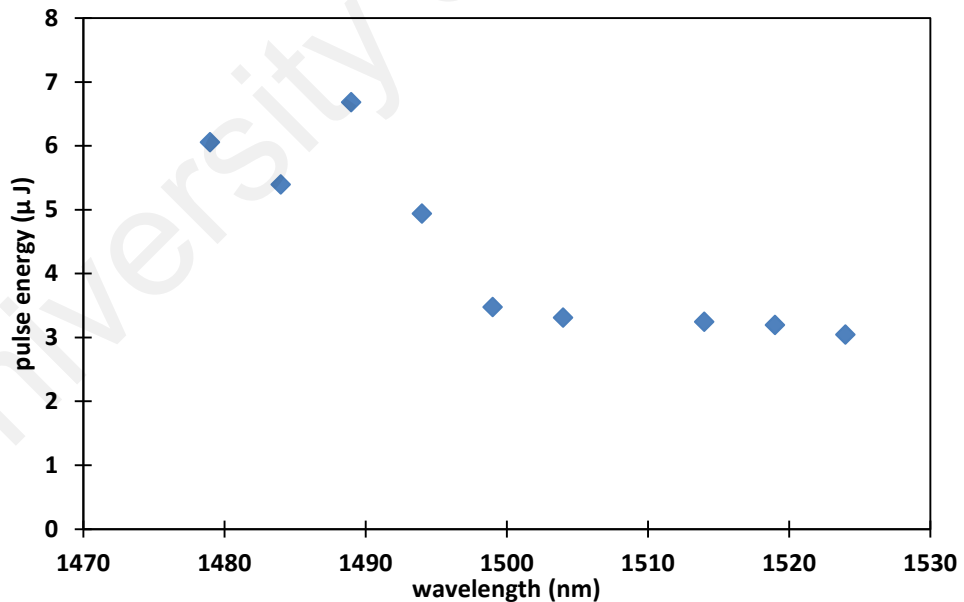


**Figure 4.7: Output pulse train at wavelength of 1509 nm with repetition rate value of 26.5 kHz**

The pulse energy of the tunable Q-switched S- band fiber laser pulses against the wavelength is shown in Figure 4.8. These values are obtained from the relationship between the average output power and the pulse repetition rate, such that the value of the pulse energy ( $E_p$ ) is given by the value of the average output power ( $P$ ) over pulse repetition rate ( $V$ ) which enable the calculation of pulse energy by (Petkov, 2014):

$$E_p = \frac{P}{V} \quad 4.1$$

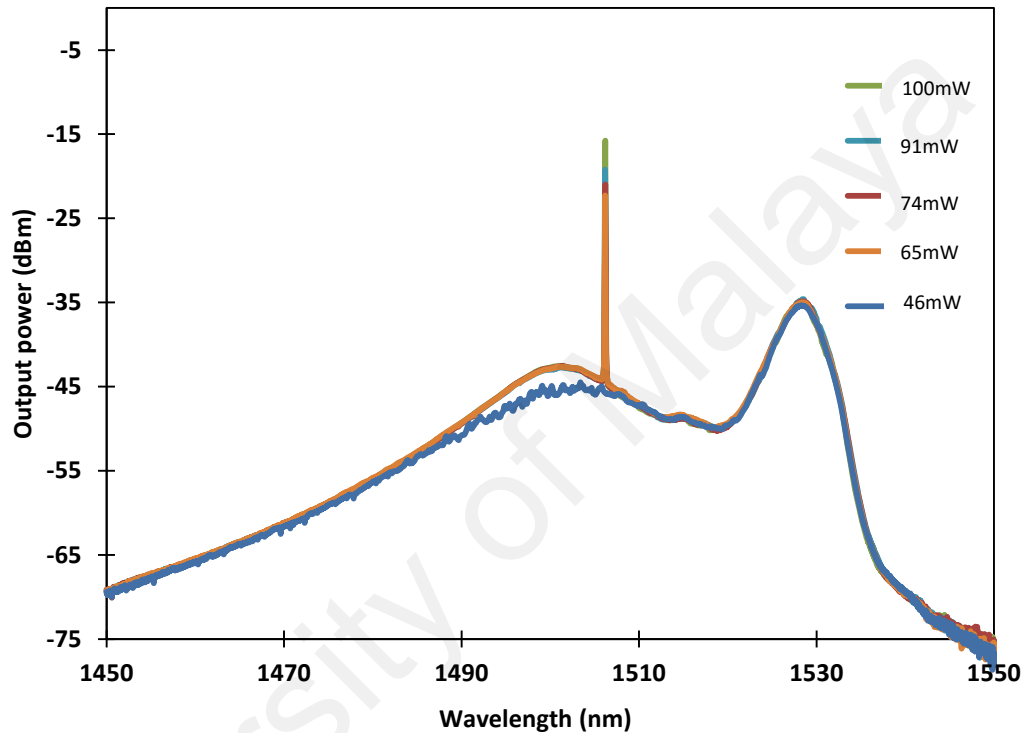
From the graph in Figure 4.8, it is observed that the pulse energy decreases from 6.1  $\mu\text{J}$  at wavelength of 1479 nm to a minimum value of 3.0  $\mu\text{J}$  at 1524 nm. The pulse energy decreases largely from 6.7  $\mu\text{J}$  to 4.9  $\mu\text{J}$  at the wavelength 1489 to 1494 nm. All the pulse energy results are taken at the maximum pump power of  $\sim 100$  mW.



**Figure 4.8: Pulse Energy against wavelength**

#### 4.4 SLM Distributed Bragg Reflector Fiber Laser using DC-EDF

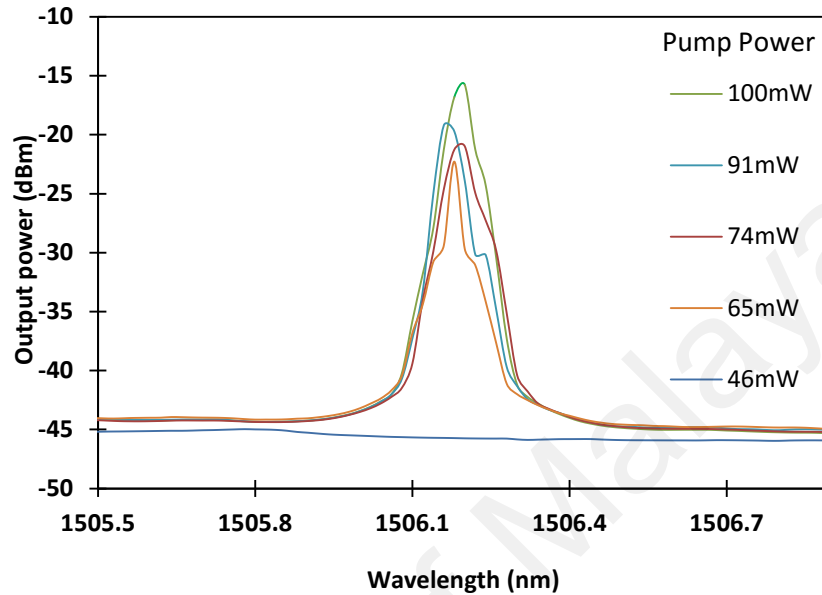
Figure 4.9 shows the output spectrum of the SLM DBR fiber laser taken from the OSA, with a spectral resolution of 0.02 nm at five different pump powers. From the figure, it shows the laser outputs over a broad ASE spectrum that covers a wavelength range from about 1450 nm to 1550 nm.



**Figure 4.9: Output spectrum of the SLM DBR fiber laser with different pump power**

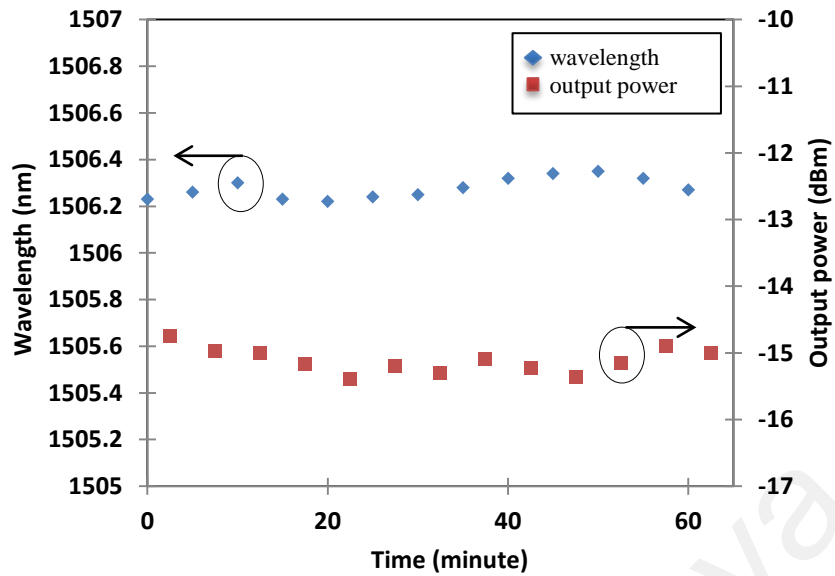
Figure 4.10 shows the zoomed-in view of the spectrum in Figure 4.9. As presented in Figure 4.10, lasing is not initiated until the pump power of 65mW is reached, whereupon continuous wave (CW) laser operation in the fiber laser is first observed with output power amplitude of about -22 dBm. Output power amplitude increases as the pump power is increased, from -19 dBm at pump power of 74 mW to a maximum value of -15 dBm at 100 mW pump power. This output power is limited only by the available pump power, insofar as it is expected that higher output power amplitude could be achieved by further increasing the pump power. As for the case of the 3 dB bandwidth of the laser spectrum, values measured at pump power of 65 mW, 74 mW,

91 mW, and 100 mW are 0.04 nm, 0.02 nm, 0.06 nm and 0.04 nm respectively. This indicates that the system is capable of generating a narrow spectral width below 0.06 nm.



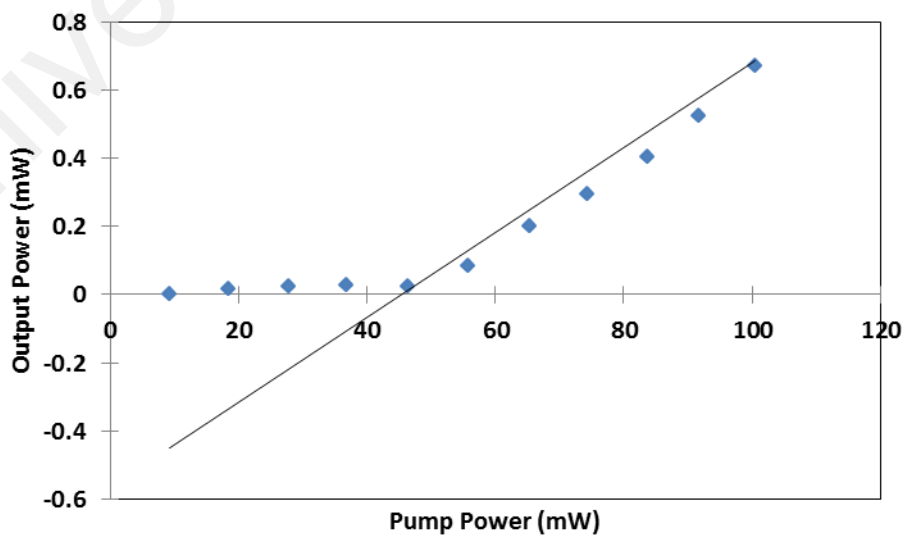
**Figure 4.10: Zoom in view of output spectrum in Figure 4.9**

To investigate and verify the stability of the output laser in this research work, a short-term stability measurement of the output spectrum at the pump power of 100 mW is carried out. The stability of the output laser in terms of output power amplitude and central wavelength of the fiber laser is plotted in the graph shown in Figure 4.11. The observation time is over 60 minutes at the lasing wavelength of 1506.2 nm with an initial output power of approximately -15 dBm. The central wavelength of 1506.2 nm with the output power of approximately -15 dBm shows no significant variation in terms of wavelength and output power within the observation time. These power and wavelength variations are observed to be less than 0.5 dB and 0.13 nm respectively. This provides clear evidence that the output stability of the proposed fiber laser is well maintained over time.



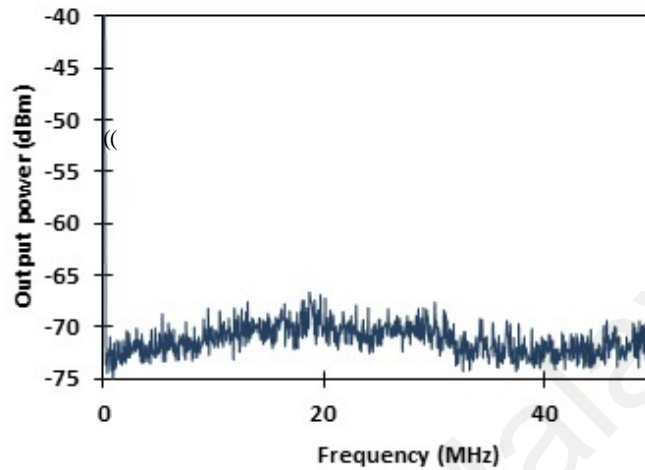
**Figure 4.11: Stability measurement of the output laser**

Figure 4.12 shows the average output power against a 980 nm pump power. Lasing threshold power can be deduced from the figure to be approximately 50 mW, with an almost linear increment. The laser output slope efficiency above the threshold value is about 0.01%. Even at the maximum pump power of 100.4 mW, the measured output power, with a value of 0.7 mW, has not reached its saturation value yet. These results indicate that higher output powers are achievable within this system.



**Figure 4.12: Average output power against pump power at wavelength 1506.2nm**

Figure 4.13 shows the laser output as observed from the RFSA across an approximate 0 - 50 MHz frequency span. The absence of an observed beat frequency provides verification that the laser is operating in single longitudinal mode (SLM).



**Figure 4.13: RFSA spectrum of the output laser by the SLM DBR fiber laser setup**

Further verification of the SLM operation of this system is achieved by using the delayed self-heterodyned technique. The technique used Mach-Zehnder interferometer (MZI) configuration (Canagasabey et al., 2011), as shown in Figure 4.14 that consists of single longitudinal mode-fiber laser, 3dB coupler, 500 m long single mode fiber (SMF), Polarization Controller (PC) and acousto-optic modulator (AOM). A basic MZI configuration is constructed using two coupler, one at the input that acts as splitter and another at the output that acts as combiner. The light is split in two arms of the interferometer by the input coupler and recombined at the output by the output coupler. The optical path length of two arms is unequal making the phase shift corresponding to delay to be a function of wavelength of the input signal (Mehra, Shahani, & Khan, 2014). In this setup, the input coupler divides the signal from the fiber laser into two portions of the same power, with one portion propagating into the 500 m long SMF, while the other portion propagates into the AOM, which operates at 80 MHz. Both

signals are then recombined at the output coupler (Derickson, 1998; F. Muhammad, Zulkifl, Latif, Harun, & Ahmad, 2012). The line-width spectrum obtained from this measurement is shown in Figure 4.15, whereupon it can be observed that a small line-width value of 20 kHz has been achieved in this system. This characteristic is relatively smaller than that reported in (H. Ahmad, Zulkifli, Latif, et al., 2012), in which the SLM S-band fiber laser is realized using a ring cavity configuration.

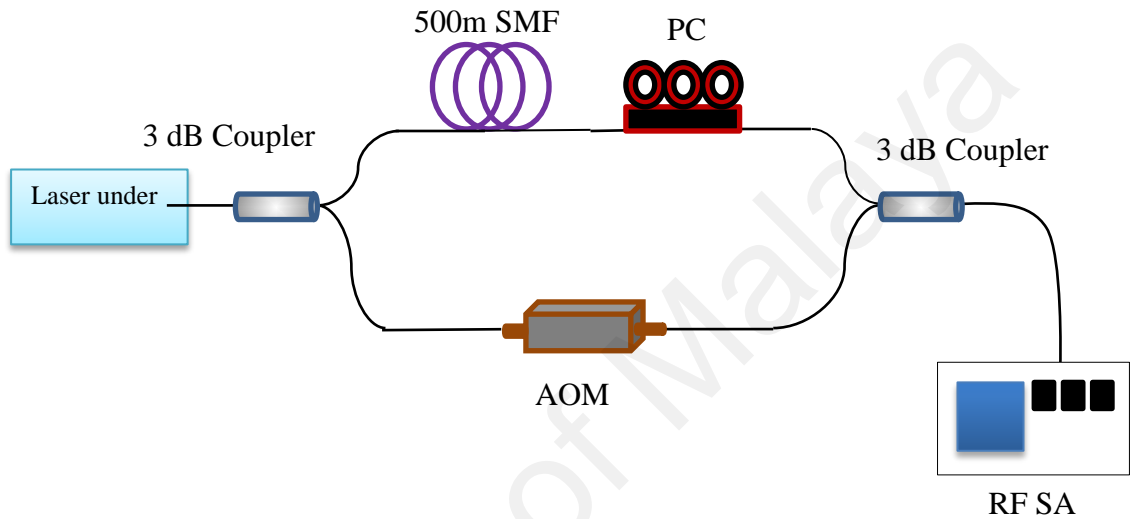


**Figure 4.14: Delayed self-heterodyne technique using a Mach-Zehnder interferometer (MZI)**

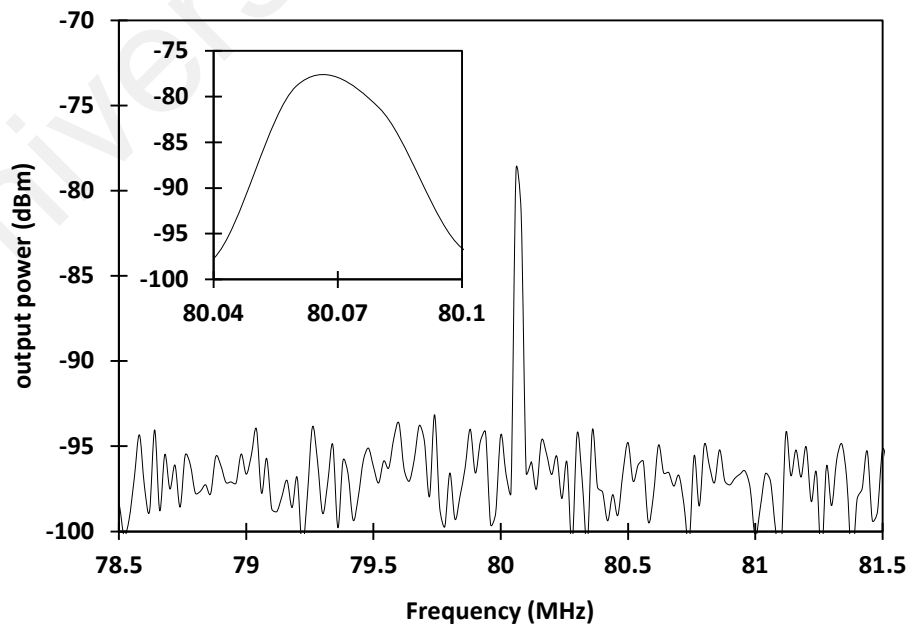


**Figure 4.15: RF spectrum of delayed self-heterodyne signal**

## CHAPTER 5: CONCLUSION

### 5.1 Conclusion

In conclusion, the research work has been able to achieve its primary objectives; to propose and demonstrate pulsed operation in depressed-cladding erbium doped fiber laser and to study the wavelength range tunability of Q-switched operation in the S-band region. . A wideband tunable CNT-based Q-Switched fiber laser operating in the S-band region using a tunable Fabry-Perot etalon filter as the wavelength tuning and filtering mechanism is proposed and demonstrated. The system uses a 15 m long Depressed Cladding-Erbium Doped Fiber (DC-EDF) laser as the gain medium, while a thin CNT film is sandwiched between two connectors to function as the Saturable absorber for the generation of the desired Q-switched pulses. The tuning range of the laser output carrying the Q-switching pulses covers a wide wavelength range of 47 nm, which spans from 1479 nm to 1526 nm. The lasing and Q-switching thresholds have a respective value of ~36 mW and ~65 mW. A repetition rate of 24.4 kHz is obtained at the maximum pump power of 100.4 mW at the wavelength of 1498 nm, together with pulse width and pulse energy of 1.2  $\mu$ s and 26.1 nJ respectively. In addition to the DC-EDF, the generation of single longitudinal mode using DC-EDF is also further expanded into the study of DC-EDF.

### 5.2 Future works

The significance of this work is that a wideband tunable Q-switched pulse has been realized in a band different from the ordinary C-band region, which is the S-band region, by using the Fabry-Perot etalon filter as the wavelength tuning mechanism. The use of Fabry-Perot etalon filter in achieving tunable Q-switched fiber laser in this work proves that even with the incorporation of the filter in the cavity, the Q-switched pulse operation can still be conserved, though the use of the filter itself could not be justified novelty. The Fabry-Perot etalon filter can be tuned manually by adjusting the voltage

supplied to the filter from the smallest scale of 0.1 V, the wavelength shift is dependent on the resolution of the applied voltage. By careful tuning of the filter, a smaller wavelength shift of less than 0.5 nm could be attained. For future work, a higher output power of DC-EDF with backward pumping is needed to produce high power fiber laser especially in the S-band region.

University of Malaya

## REFERENCES

- Agrawal, G. (2010). *Applications of nonlinear fiber optics*: Academic press.
- Agrawal, G. P. (2005). *Lightwave technology: telecommunication systems*: John Wiley & Sons.
- Ahmad, F., Harun, S., Nor, R., Zulkepely, N., Muhammad, F., Arof, H., & Ahmad, H. (2014). Mode-locked soliton erbium-doped fiber laser using a single-walled carbon nanotubes embedded in polyethylene oxide thin film saturable absorber. *Journal of Modern Optics*, 61(6), 541-545.
- Ahmad, H., Saat, N., & Harun, S. (2005). S-band erbium-doped fiber ring laser using a fiber Bragg grating. *Laser Physics Letters*, 2(7), 369.
- Ahmad, H., Zulkifli, M., Latif, A., Jemangin, M., Chong, S., & Harun, S. (2012). Tunable single longitudinal mode S-band fiber laser using a 3 m length of erbium-doped fiber. *Journal of Modern Optics*, 59(3), 268-273.
- Ahmad, H., Zulkifli, M., Muhammad, F., Jemangin, M., Dimyati, K., Pal, B., & Harun, S. (2012). Passively Q-Switched 11-Channel Stable Brillouin Erbium-Doped Fiber Laser With Graphene as the Saturable Absorber. *Photonics Journal, IEEE*, 4(5), 2050-2056.
- Ahmad, H., Zulkifli, M., Muhammad, F., Zulkifli, A., & Harun, S. (2013). Tunable graphene-based Q-switched erbium-doped fiber laser using fiber Bragg grating. *Journal of Modern Optics*, 60(3), 202-212.
- Ahmed, M., Ali, N., Salleh, Z., Rahman, A., Harun, S., Manaf, M., & Arof, H. (2014). All fiber mode-locked Erbium-doped fiber laser using single-walled carbon nanotubes embedded into polyvinyl alcohol film as saturable absorber. *Optics & Laser Technology*, 62, 40-43.
- Amemiya, T., & Nakano, Y. (2010). *Single Mode Operation of 1.5- $\mu$ m Waveguide Optical Isolators Based on the Nonreciprocal-loss Phenomenon*: INTECH Open Access Publisher.
- Arbore, M., & Keaton, G. (2003). Fiber amplifiers with depressed cladding and their uses in Er-doped fiber amplifiers for the S-band: Google Patents.
- Arbore, M. A. (2005, 2005/03/06). *Application of Fundamental-Mode Cutoff for Novel Amplifiers and Lasers*. Paper presented at the Optical Fiber Communication Conference and Exposition and The National Fiber Optic Engineers Conference, Anaheim, California.
- Arbore, M. A. (2005). Communication system using S-band Er-doped fiber amplifiers with depressed cladding: Google Patents.
- Arbore, M. A., Zhou, Y., & Kmetec, J. D. (2005). S-band light sources using erbium-doped fiber with depressed cladding: Google Patents.

- Avouris, P., Freitag, M., & Perebeinos, V. (2008). Carbon-nanotube photonics and optoelectronics. *Nature Photonics*, 2(6), 341-350.
- Bachilo, S. M., Strano, M. S., Kittrell, C., Hauge, R. H., Smalley, R. E., & Weisman, R. B. (2002). Structure-assigned optical spectra of single-walled carbon nanotubes. *Science*, 298(5602), 2361-2366.
- Bellemare, A., Karbsek, M., Riviere, C., Babin, F., He, G., Roy, V., & Schinn, G. W. (2001). A broadly tunable erbium-doped fiber ring laser: experimentation and modeling. *Selected Topics in Quantum Electronics, IEEE Journal of*, 7(1), 22-29.
- Bellouard, Y., & Hongler, M.-O. (2011). Femtosecond-laser generation of self-organized bubble patterns in fused silica. *Optics Express*, 19(7), 6807-6821.
- Buck, J. A. (2004). *Fundamentals of optical fibers*: John Wiley & Sons.
- Canagasabay, A., Michie, A., Canning, J., Holdsworth, J., Fleming, S., Wang, H.-C., & Åslund, M. L. (2011). A comparison of delayed self-heterodyne interference measurement of laser linewidth using Mach-Zehnder and Michelson Interferometers. *Sensors*, 11(10), 9233-9241.
- Cao, W., Wang, H., Luo, A., Luo, Z., & Xu, W. (2012). Graphene-based, 50 nm wide-band tunable passively Q-switched fiber laser. *Laser Physics Letters*, 9(1), 54.
- Chang, H. X., Sun, Z. H., Yuan, Q. H., Ding, F., Tao, X. M., Yan, F., & Zheng, Z. J. (2010). Thin Film Field-Effect Phototransistors from Bandgap-Tunable, Solution-Processed, Few-Layer Reduced Graphene Oxide Films. *Advanced Materials*, 22(43), 4872-+. doi: DOI 10.1002/adma.201002229
- Chen, Y.-C., Raravikar, N., Schadler, L., Ajayan, P., Zhao, Y.-P., Lu, T.-M., . . . Zhang, X.-C. (2002). Ultrafast optical switching properties of single-wall carbon nanotube polymer composites at 1.55  $\mu\text{m}$ . *Applied Physics Letters*, 81(6), 975-977.
- Chong, A., Buckley, J., Renninger, W., & Wise, F. (2006). All-normal-dispersion femtosecond fiber laser. *Optics Express*, 14(21), 10095-10100.
- Chong, A., Renninger, W. H., & Wise, F. W. (2007). All-normal-dispersion femtosecond fiber laser with pulse energy above 20nJ. *Optics letters*, 32(16), 2408-2410.
- Chou, S., Plentz, F., Jiang, J., Saito, R., Nezich, D., Ribeiro, H., . . . Santos, A. (2005). Phonon-assisted excitonic recombination channels observed in DNA-wrapped carbon nanotubes using photoluminescence spectroscopy. *Physical review letters*, 94(12), 127402.
- Coddington, I., Swann, W. C., & Newbury, N. R. (2008). Coherent multiheterodyne spectroscopy using stabilized optical frequency combs. *Physical review letters*, 100(1), 013902.

- Davis, K. M., Miura, K., Sugimoto, N., & Hirao, K. (1996). Writing waveguides in glass with a femtosecond laser. *Optics letters*, 21(21), 1729-1731.
- Derickson, D. (1998). *Fiber optic test and measurement*. Paper presented at the Fiber optic test and measurement/edited by Dennis Derickson. Upper Saddle River, NJ: Prentice Hall, c1998.
- Digonnet, M. J. (2001). *Rare-earth-doped fiber lasers and amplifiers, revised and expanded*: CRC press.
- Dong, B., Hao, J., Hu, J., & Liaw, C.-y. (2011). Short linear-cavity Q-switched fiber laser with a compact short carbon nanotube based saturable absorber. *Optical Fiber Technology*, 17(2), 105-107.
- Dong, B., Hu, J., Liaw, C.-Y., Hao, J., & Yu, C. (2011). Wideband-tunable nanotube Q-switched low threshold erbium doped fiber laser. *Applied Optics*, 50(10), 1442-1445.
- Dong, B., Hu, J. H., Liaw, C. Y., Hao, J. Z., & Yu, C. Y. (2011). Wideband-tunable nanotube Q-switched low threshold erbium doped fiber laser. *Applied Optics*, 50(10), 1442-1445. doi: Doi 10.1364/Ao.50.001442
- Dong, J. L., Xu, W. C., Luo, Z. C., Luo, A. P., Wang, H. Y., Cao, W. J., & Wang, L. Y. (2011). Tunable and switchable dual-wavelength passively mode-locked fiber ring laser with high-energy pulses at a sub-100 kHz repetition rate. *Optics Communications*, 284(24), 5719-5722. doi: DOI 10.1016/j.optcom.2011.07.078
- Dong, L., Li, J., McKay, H., Marcinkevicius, A., Thomas, B., Moore, M., . . . Fermann, M. E. (2008). *Robust and Practical Optical Fibers for Single Mode Operation with Core Diameters up to 170? m*. Paper presented at the Conference on Lasers and Electro-Optics.
- Eidam, T., Hanf, S., Seise, E., Andersen, T. V., Gabler, T., Wirth, C., . . . Tünnermann, A. (2010). Femtosecond fiber CPA system emitting 830 W average output power. *Optics letters*, 35(2), 94-96.
- Erdogan, T. (1997). Fiber grating spectra. *Lightwave Technology, Journal of*, 15(8), 1277-1294.
- Fermann, M. E., Galvanauskas, A., & Sucha, G. (2002). *Ultrafast lasers: Technology and applications* (Vol. 80): CRC Press.
- Fermann, M. E., & Hartl, I. (2009). Ultrafast fiber laser technology. *Selected Topics in Quantum Electronics, IEEE Journal of*, 15(1), 191-206.
- Foroni, M., Poli, F., Ruggeri, L., Selleri, S., Cucinotta, A., & Vavassori, P. (2005). Bending influence on depressed-cladding EDFA gain spectrum. *2005 7th International Conference on Transparent Optical Networks, Vol 2, Proceedings*, 351-354.

- Garnov, S., Konov, V., Kononenko, T., Pashinin, V., & Sinyavsky, M. (2004). Microsecond Laser Material Processing at 1.06  $\mu\text{m}$ . *LASER PHYSICS-LAWRENCE-*, 14(6), 910-915.
- Gattass, R. R., & Mazur, E. (2008). Femtosecond laser micromachining in transparent materials. *Nature Photonics*, 2(4), 219-225.
- Glezer, E. N., & Mazur, E. (1997). Ultrafast-laser driven micro-explosions in transparent materials. *Applied Physics Letters*, 71(7), 882-884.
- Gomes, L. A., Orsila, L., Jouhti, T., & Okhotnikov, O. G. (2004). Picosecond SESAM-based ytterbium mode-locked fiber lasers. *Selected Topics in Quantum Electronics, IEEE Journal of*, 10(1), 129-136.
- Han, M., Zhang, S., Li, X., Zhang, H., Wen, F., & Yang, Z. (2014). High-energy, tunable-wavelengths, Q-switched pulse laser. *Optics Communications*, 326, 24-28.
- Hartl, I., Marcinkevicius, A., McKay, H., Dong, L., & Fermann, M. (2009). *Multi-core leakage-channel fiber for coherent beam combining*. Paper presented at the Proc. Photon. West Conf., San Jose, CA.
- Harun, S. W., Dimiyati, K., Jayapalan, K. K., & Ahmad, H. (2007). An overview on S-band erbium-doped fiber amplifiers. *Laser Physics Letters*, 4(1), 10-15.
- Hasan, T., Sun, Z., Wang, F., Bonaccorso, F., Tan, P. H., Rozhin, A. G., & Ferrari, A. C. (2009). Nanotube-polymer composites for ultrafast photonics. *Adv. Mater*, 21(38-39), 3874-3899.
- Hausken, T. (2008). Incumbent sources resist fibre laser proliferation. *Optics and Laser Europe*, 157, 31-34.
- Headley, C., & Agrawal, G. (2005). *Raman amplification in fiber optical communication systems*: Academic Press.
- Hill, K., Fujii, Y., Johnson, D. C., & Kawasaki, B. (1978). Photosensitivity in optical fiber waveguides: Application to reflection filter fabrication. *Applied Physics Letters*, 32(10), 647-649.
- Hill, K. O., & Meltz, G. (1997). Fiber Bragg grating technology fundamentals and overview. *Journal of lightwave technology*, 15(8), 1263-1276.
- Iijima, S. (1991). Helical microtubules of graphitic carbon. *Nature*, 354(6348), 56-58.
- Ishio, H., Minowa, J., & Nosu, K. (1984). Review and status of wavelength-division-multiplexing technology and its application. *Journal of lightwave technology*, 2, 448-463.
- Jeong, H., Choi, S. Y., Rotermund, F., Cha, Y.-H., Jeong, D.-Y., & Yeom, D.-I. (2014). All-fiber mode-locked laser oscillator with pulse energy of 34 nJ using a single-walled carbon nanotube saturable absorber. *Optics Express*, 22(19), 22667-22672.

- Jeong, Y. e., Sahu, J., Payne, D., & Nilsson, J. (2004). Ytterbium-doped large-core fiber laser with 1.36 kW continuous-wave output power. *Optics Express*, 12(25), 6088-6092.
- Jung, M., Koo, J., Chang, Y., Debnath, P., Song, Y., & Lee, J. (2012). An all fiberized, 1.89- $\mu\text{m}$  Q-switched laser employing carbon nanotube evanescent field interaction. *Laser Physics Letters*, 9(9), 669.
- Kamlage, G., Bauer, T., Ostendorf, A., & Chichkov, B. (2003). Deep drilling of metals by femtosecond laser pulses. *Applied Physics A*, 77(2), 307-310.
- Kashiwagi, K., Yamashita, S., & Set, S. Y. (2007). *Optical Reflectometry for; in-situ Monitoring of Carbon Nanotubes Deposition by Optical Tweezers*. Paper presented at the Conference on Lasers and Electro-Optics.
- Kashyap, R. (2013). The Fiber Fuse-from a curious effect to a critical issue: A 25 th year retrospective. *Optics Express*, 21(5), 6422-6441.
- Kasim, N., Anyi, C. L., Haris, H., Ahmad, F., Ali, N. M., Ahmad, H., . . . Harun, S. W. (2014). Q-switched erbium-doped fiber laser using multi-layer graphene based saturable absorber. *Journal of Nonlinear Optical Physics & Materials*, 23(1). doi: Artn 1450009
- Doi 10.1142/S021886351450009x
- Kataura, H., Kumazawa, Y., Maniwa, Y., Ohtsuka, Y., Sen, R., Suzuki, S., & Achiba, Y. (2000). Diameter control of single-walled carbon nanotubes. *Carbon*, 38(11), 1691-1697.
- Kataura, H., Kumazawa, Y., Maniwa, Y., Umezue, I., Suzuki, S., Ohtsuka, Y., & Achiba, Y. (1999). Optical properties of single-wall carbon nanotubes. *Synthetic metals*, 103(1), 2555-2558.
- Kawasaki, B. S., Hill, K. O., Johnson, D. C., & Fujii, Y. (1978). Narrow-band Bragg reflectors in optical fibers. *Optics letters*, 3(2), 66-68.
- Keilmann, F., Gohle, C., & Holzwarth, R. (2004). Time-domain mid-infrared frequency-comb spectrometer. *Optics letters*, 29(13), 1542-1544.
- Keiser, G. E. (1999). A review of WDM technology and applications. *Optical Fiber Technology*, 5(1), 3-39.
- Keller, U. (2010). Ultrafast solid-state laser oscillators: a success story for the last 20 years with no end in sight. *Applied Physics B*, 100(1), 15-28.
- Keller, U., Weingarten, K. J., Kartner, F. X., Kopf, D., Braun, B., Jung, I. D., . . . derAu, J. A. (1996). Semiconductor saturable absorber mirrors (SESAM's) for femtosecond to nanosecond pulse generation in solid-state lasers. *Ieee Journal of Selected Topics in Quantum Electronics*, 2(3), 435-453. doi: Doi 10.1109/2944.571743

- Kieu, K., & Wise, F. (2009). Soliton thulium-doped fiber laser with carbon nanotube saturable absorber. *IEEE photonics technology letters: a publication of the IEEE Laser and Electro-optics Society*, 21(3), 128.
- Kivistö, S., Hakulinen, T., Guina, M., Rößner, K., Forchel, A., & Okhotnikov, O. (2008). 2 Watt 2  $\mu\text{m}$  Tm/Ho fiber laser system passively Q-switched by antimonide semiconductor saturable absorber. Paper presented at the Photonics Europe.
- Kivistö, S., Hakulinen, T., Kaskela, A., Aitchison, B., Brown, D. P., Nasibulin, A. G., . . . Okhotnikov, O. G. (2009). Carbon nanotube films for ultrafast broadband technology. *Optics Express*, 17(4), 2358-2363.
- Kracht, D., & Brinkmann, R. (2004). Green Q-switched microsecond laser pulses by overcoupled intracavity second harmonic generation. *Optics Communications*, 231(1), 319-324.
- Lam, D., & Garside, B. K. (1981). Characterization of single-mode optical fiber filters. *Applied Optics*, 20(3), 440-445.
- Lebedkin, S., Hennrich, F., Kiowski, O., & Kappes, M. M. (2008). Photophysics of carbon nanotubes in organic polymer-toluene dispersions: Emission and excitation satellites and relaxation pathways. *Physical Review B*, 77(16), 165429.
- Lebedkin, S., Schweiss, P., Renker, B., Malik, S., Hennrich, F., Neumaier, M., . . . Kappes, M. M. (2002). Single-wall carbon nanotubes with diameters approaching 6 nm obtained by laser vaporization. *Carbon*, 40(3), 417-423.
- Lefebvre, J., & Finnie, P. (2008). Excited excitonic states in single-walled carbon nanotubes. *Nano letters*, 8(7), 1890-1895.
- Li, J. F., Luo, H. Y., He, Y. L., Liu, Y., Zhang, L., Zhou, K. M., . . . Turistyn, S. K. (2014). Semiconductor saturable absorber mirror passively Q-switched 2.97  $\mu\text{m}$  fluoride fiber laser. *Laser Physics Letters*, 11(6). doi: Artn 065102
- Doi 10.1088/1612-2011/11/6/065102
- Li, X. L., Xu, J. L., Wu, Y. Z., He, J. L., & Hao, X. P. (2011). Large energy laser pulses with high repetition rate by graphene Q-switched solid-state laser. *Optics Express*, 19(10), 9950-9955.
- Limpert, J., Roser, F., Schreiber, T., & Tunnermann, A. (2006). High-power ultrafast fiber laser systems. *Ieee Journal of Selected Topics in Quantum Electronics*, 12(2), 233.
- Liu, X., Si, J., Chang, B., Xu, G., Yang, Q., Pan, Z., . . . Wan, M. (1999). Third-order optical nonlinearity of the carbon nanotubes. *Applied Physics Letters*, 74(2), 164-166.

- Margulis, V. A., & Sizikova, T. (1998). Theoretical study of third-order nonlinear optical response of semiconductor carbon nanotubes. *Physica B: Condensed Matter*, 245(2), 173-189.
- Martinez, A., & Yamashita, S. (2011). *Carbon nanotube-based photonic devices: Applications in nonlinear optics*: INTECH Open Access Publisher.
- Mary, R., Beecher, S., Brown, G., Thomson, R., Jaque, D., Ohara, S., & Kar, A. (2012). Compact, highly efficient ytterbium doped bismuthate glass waveguide laser. *Optics letters*, 37(10), 1691-1693.
- Mary, R., Choudhury, D., & Kar, A. K. (2014). Applications of fiber lasers for the development of compact photonic devices. *Selected Topics in Quantum Electronics, IEEE Journal of*, 20(5), 72-84.
- Masson, J., St-Gelais, R., Poulin, A., & Peter, Y.-A. (2010). Tunable fiber laser using a MEMS-based in plane Fabry-Pérot filter. *Quantum Electronics, IEEE Journal of*, 46(9), 1313-1319.
- Maultzsch, J., Pomraenke, R., Reich, S., Chang, E., Prezzi, D., Ruini, A., . . . Lienau, C. (2005). Exciton binding energies in carbon nanotubes from two-photon photoluminescence. *Physical Review B*, 72(24), 241402.
- Mears, R. J., Reekie, L., Poole, S., & Payne, D. N. (1985). Neodymium-doped silica single-mode fibre lasers. *Electronics Letters*, 21(17), 738-740.
- Mehra, R., Shahani, H., & Khan, A. (2014). Mach Zehnder Interferometer and its Applications. *Int. J. Comput. Appl*, 31-36.
- Meltz, G., Morey, W. W., & Glenn, W. (1989). Formation of Bragg gratings in optical fibers by a transverse holographic method. *Optics letters*, 14(15), 823-825.
- Moeller, G. K. (1969). 10.6 MICRON CARBON DIOXIDE LASER WITH HELIUM ADDED: US Patent 3,464,028.
- Mortimore, D. B. (1988). Fiber loop reflectors. *Lightwave Technology, Journal of*, 6(7), 1217-1224.
- Muhammad, F., Zulkifl, M., Latif, A., Harun, S., & Ahmad, H. (2012). Graphene-based saturable absorber for single-longitudinal-mode operation of highly doped erbium-doped fiber laser. *Photonics Journal, IEEE*, 4(2), 467-475.
- Muhammad, F. D., Zulkifli, M. Z., & Ahmad, H. (2014). Graphene based Q-switched tunable S-band fiber laser incorporating arrayed waveguide gratings (AWG). *Journal of Nonlinear Optical Physics & Materials*, 23(1). doi: Artn 1450004
- Doi 10.1142/S0218863514500040
- Nanotubes, C. (2001). Synthesis, Structure, Properties, and Applications. *Topics in applied physics*, 80, 113-146.

- Nicholson, J., Windeler, R., & DiGiovanni, D. (2007). Optically driven deposition of single-walled carbon-nanotube saturable absorbers on optical fiber end-faces. *Optics Express*, 15(15), 9176-9183.
- Nikolaev, S. V., Pozhar, V. V. e., & Dzyubenko, M. I. (2006). Generation of microsecond laser pulses in polyurethane matrices doped with dyes. *Quantum electronics*, 36(8), 758-762.
- O'connell, M. J., Bachilo, S. M., Huffman, C. B., Moore, V. C., Strano, M. S., Haroz, E. H., . . . Kittrell, C. (2002). Band gap fluorescence from individual single-walled carbon nanotubes. *Science*, 297(5581), 593-596.
- Paschotta, R., Häring, R., Gini, E., Melchior, H., Keller, U., Offerhaus, H., & Richardson, D. (1999). Passively Q-switched 0.1-mJ fiber laser system at 1.53  $\mu\text{m}$ . *Optics letters*, 24(6), 388-390.
- Perebeinos, V., Tersoff, J., & Avouris, P. (2005). Effect of exciton-phonon coupling in the calculated optical absorption of carbon nanotubes. *Physical review letters*, 94(2), 027402.
- Petkov, P. (2014). Factors influencing laser material removal process in micro cavity manufacturing. *KES Trans. Sustain. Des. Manufact*, 1, 973-984.
- Pinto, A. M., & Lopez-Amo, M. (2013). All-fiber lasers through photonic crystal fibers. *Nanophotonics*, 2(5-6), 355-368.
- Plentz, F., Ribeiro, H. B., Jorio, A., Strano, M. S., & Pimenta, M. A. (2005). Direct experimental evidence of exciton-phonon bound states in carbon nanotubes. *Physical review letters*, 95(24), 247401.
- Popa, D., Sun, Z., Hasan, T., Torrisi, F., Wang, F., & Ferrari, A. C. (2011). Graphene Q-switched, tunable fiber laser. *Applied Physics Letters*, 98(7). doi: Artn 073106  
Doi 10.1063/1.3552684
- Popa, D., Sun, Z., Torrisi, F., Hasan, T., Wang, F., & Ferrari, A. C. (2010). Sub 200 fs pulse generation from a graphene mode-locked fiber laser. *Applied Physics Letters*, 97(20). doi: Artn 203106  
Doi 10.1063/1.3517251
- Reich, S., Thomsen, C., & Robertson, J. (2005). Exciton resonances quench the photoluminescence of zigzag carbon nanotubes. *Physical review letters*, 95(7), 077402.
- Rozhin, A., Scardaci, V., Wang, F., Hennrich, F., White, I., Milne, W., & Ferrari, A. (2006). Generation of ultra-fast laser pulses using nanotube mode-lockers. *physica status solidi (b)*, 243(13), 3551-3555.
- Saito, R., Fujita, M., Dresselhaus, G., & Dresselhaus, u. M. (1992). Electronic structure of chiral graphene tubules. *Applied Physics Letters*, 60(18), 2204-2206.

- Sakakibara, Y., Tatsuura, S., Kataura, H., Tokumoto, M., & Achiba, Y. (2003). Near-infrared saturable absorption of single-wall carbon nanotubes prepared by laser ablation method. *Japanese journal of applied physics*, 42(5A), L494.
- Samson, B., Carter, A., & Tankala, K. (2011). Doped fibres: Rare-earth fibres power up. *Nature Photonics*, 5(8), 466-467.
- Schaffer, C. B., Brodeur, A., & Mazur, E. (2001). Laser-induced breakdown and damage in bulk transparent materials induced by tightly focused femtosecond laser pulses. *Measurement Science and Technology*, 12(11), 1784.
- Schaffer, C. B., Jamison, A. O., & Mazur, E. (2004). Morphology of femtosecond laser-induced structural changes in bulk transparent materials. *Applied Physics Letters*, 84(9), 1441-1443.
- Schoonderbeek, A., Schuetz, V., Haupt, O., & Stute, U. (2010). Laser processing of thin films for photovoltaic applications. *Journal of Laser Micro/Nanoengineering*, 5(3), 248-255.
- Set, S. Y., Yaguchi, H., Tanaka, Y., & Jablonski, M. (2004). Ultrafast fiber pulsed lasers incorporating carbon nanotubes. *Selected Topics in Quantum Electronics, IEEE Journal of*, 10(1), 137-146.
- Shanguan, H., Casperson, L. W., & Prahl, S. A. (1996). Microsecond laser ablation of thrombus and gelatin under clear liquids: Contact versus noncontact. *Selected Topics in Quantum Electronics, IEEE Journal of*, 2(4), 818-825.
- Shanguan, H., Casperson, L. W., Shearin, A., Gregory, K. W., & Prahl, S. A. (1996). Drug delivery with microsecond laser pulses into gelatin. *Applied Optics*, 35(19), 3347-3357.
- Siniaeva, M., Siniavsky, M., Pashinin, V., Mamedov, A. A., Konov, V., & Kononenko, V. (2009). Laser ablation of dental materials using a microsecond Nd: YAG laser. *Laser physics*, 19(5), 1056-1060.
- Snitzer, E. (1961). Optical maser action of Nd<sup>3+</sup> in a barium crown glass. *Physical review letters*, 7(12), 444.
- Snitzer, E., Hoffman, F., & Crevier, R. (1963). *Neodymium-glass-fiber laser*. Paper presented at the JOURNAL OF THE OPTICAL SOCIETY OF AMERICA.
- Song, Y.-W., Yamashita, S., Goh, C. S., & Set, S. Y. (2007). Passively mode-locked lasers with 17.2-GHz fundamental-mode repetition rate pulsed by carbon nanotubes. *Optics letters*, 32(4), 430-432.
- Spühler, G., Paschotta, R., Fluck, R., Braun, B., Moser, M., Zhang, G., . . . Keller, U. (1999). Experimentally confirmed design guidelines for passively Q-switched microchip lasers using semiconductor saturable absorbers. *JOSA B*, 16(3), 376-388.

- Stuart, B. C., Feit, M. D., Herman, S., Rubenchik, A. M., Shore, B. W., & Perry, M. D. (1996). Optical ablation by high-power short-pulse lasers. *JOSA B*, *13*(2), 459-468.
- Sudrie, L., Franco, M., Prade, B., & Mysyrowicz, A. (2001). Study of damage in fused silica induced by ultra-short IR laser pulses. *Optics Communications*, *191*(3), 333-339.
- Sun, Z., Rozhin, A., Wang, F., Scardaci, V., Milne, W., White, I., . . . Ferrari, A. (2008). L-band ultrafast fiber laser mode locked by carbon nanotubes. *Applied Physics Letters*, *93*(6), 61114.
- Sun, Z. Z., Yan, Z., Yao, J., Beitler, E., Zhu, Y., & Tour, J. M. (2010). Growth of graphene from solid carbon sources. *Nature*, *468*(7323), 549-552. doi: Doi 10.1038/Nature09579
- Svelto, O. (1998). *Principles of Lasers*: New York Plenum Press.
- Tan, P., Hasan, T., Bonaccorso, F., Scardaci, V., Rozhin, A., Milne, W., & Ferrari, A. (2008). Optical properties of nanotube bundles by photoluminescence excitation and absorption spectroscopy. *Physica E: Low-dimensional Systems and Nanostructures*, *40*(7), 2352-2359.
- Tan, P., Rozhin, A., Hasan, T., Hu, P., Scardaci, V., Milne, W., & Ferrari, A. (2007). Photoluminescence spectroscopy of carbon nanotube bundles: Evidence for exciton energy transfer. *Physical review letters*, *99*(13), 137402.
- Taylor, R., Hnatovsky, C., & Simova, E. (2008). Applications of femtosecond laser induced self-organized planar nanocracks inside fused silica glass. *Laser & Photonics Reviews*, *2*(1-2), 26-46.
- Vaughan, M. (1989). *The Fabry-Perot interferometer: history, theory, practice and applications*: CRC press.
- Wang, F., Dukovic, G., Brus, L. E., & Heinz, T. F. (2005). The optical resonances in carbon nanotubes arise from excitons. *Science*, *308*(5723), 838-841.
- Wang, F., Rozhin, A., Scardaci, V., Sun, Z., Hennrich, F., White, I., . . . Ferrari, A. C. (2008). Wideband-tuneable, nanotube mode-locked, fibre laser. *Nature nanotechnology*, *3*(12), 738-742.
- Wang, L., Gao, C. Q., Gao, M. W., Li, Y., Yue, F. Y., Zhang, J., & Tang, D. Y. (2014). A resonantly-pumped tunable Q-switched Ho:YAG ceramic laser with diffraction-limit beam quality. *Optics Express*, *22*(1), 254-261. doi: Doi 10.1364/Oe.22.000254
- Watanabe, S., Anderson, R., Brorson, S., Dalickas, G., Fujimoto, J. G., & Flotte, T. J. (1991). Comparative studies of femtosecond to microsecond laser pulses on selective pigmented cell injury in skin. *Photochemistry and photobiology*, *53*(6), 757-762.

- Wiersma, D. S. (2008). The physics and applications of random lasers. *Nature physics*, 4(5), 359-367.
- Yamashita, S. (2012). A tutorial on nonlinear photonic applications of carbon nanotube and graphene. *Journal of lightwave technology*, 30(4), 427-447.
- Yamashita, S., Inoue, Y., Maruyama, S., Murakami, Y., Yaguchi, H., Jablonski, M., & Set, S. (2004). Saturable absorbers incorporating carbon nanotubes directly synthesized onto substrates and fibers and their application to mode-locked fiber lasers. *Optics letters*, 29(14), 1581-1583.
- Yin, S. S., & Ruffin, P. (2002). *Fiber optic sensors*: Wiley Online Library.
- Yu, Z., Wang, Y., Zhang, X., Dong, X., Tian, J., & Song, Y. (2014). A 66 fs highly stable single wall carbon nanotube mode locked fiber laser. *Laser physics*, 24(1), 015105.
- Zhao, J. Q., Wang, Y. G., Yan, P. G., Ruan, S. C., Tsang, Y. E., Zhang, G. L., & Li, H. Q. (2014). An Ytterbium-doped fiber laser with dark and Q-switched pulse generation using graphene-oxide as saturable absorber. *Optics Communications*, 312, 227-232. doi: DOI 10.1016/j.optcom.2013.09.038
- Zheng, M., Jagota, A., Strano, M. S., Santos, A. P., Barone, P., Chou, S. G., . . . Onoa, G. B. (2003). Structure-based carbon nanotube sorting by sequence-dependent DNA assembly. *Science*, 302(5650), 1545-1548.
- Zhou, D.-P., Wei, L., Dong, B., & Liu, W.-K. (2010). Tunable passively-switched erbium-doped fiber laser with carbon nanotubes as a saturable absorber. *Photonics Technology Letters, IEEE*, 22(1), 9-11.
- Zhou, D.-P., Wei, L., & Liu, W.-K. (2012). Tunable graphene Q-switched erbium-doped fiber laser with suppressed self-mode locking effect. *Applied Optics*, 51(14), 2554-2558.
- Zhou, R., Tang, P. H., Chen, Y., Chen, S. Q., Zhao, C. J., Zhang, H., & Wen, S. C. (2014). Large-energy, narrow-bandwidth laser pulse at 1645 nm in a diode-pumped Er:YAG solid-state laser passively Q-switched by a monolayer graphene saturable absorber. *Applied Optics*, 53(2), 254-258. doi: Doi 10.1364/Ao.53.000254

## LIST OF PUBLICATIONS

1. Ahmad, H., Azhari, N. S., Zulkifli, M. Z., Muhammad, F. D., & Harun, S. W. (2014). S-band SLM distributed Bragg reflector fiber laser. *Laser Physics*, 24(6), 065109
2. Poster presentation at International Seminar on Photonics, Optics, and Applications 2014, Bali Indonesia. Poster entitle “Graphene Based Mode-Locked using Fiber Bragg Grating”
3. Poster presentation at 10th International Symposium on Modern Optics and Its Applications 2015, Bandung Indonesia. Poster entitle “Wideband tunable CNT-based Q-switched S-band fiber laser using tunable Fabry-Perot etalon filter”

# **APPENDICES**

University of Malaya